Model-free motion control of positioning stage

Xiao Zhang

Master of Science Thesis

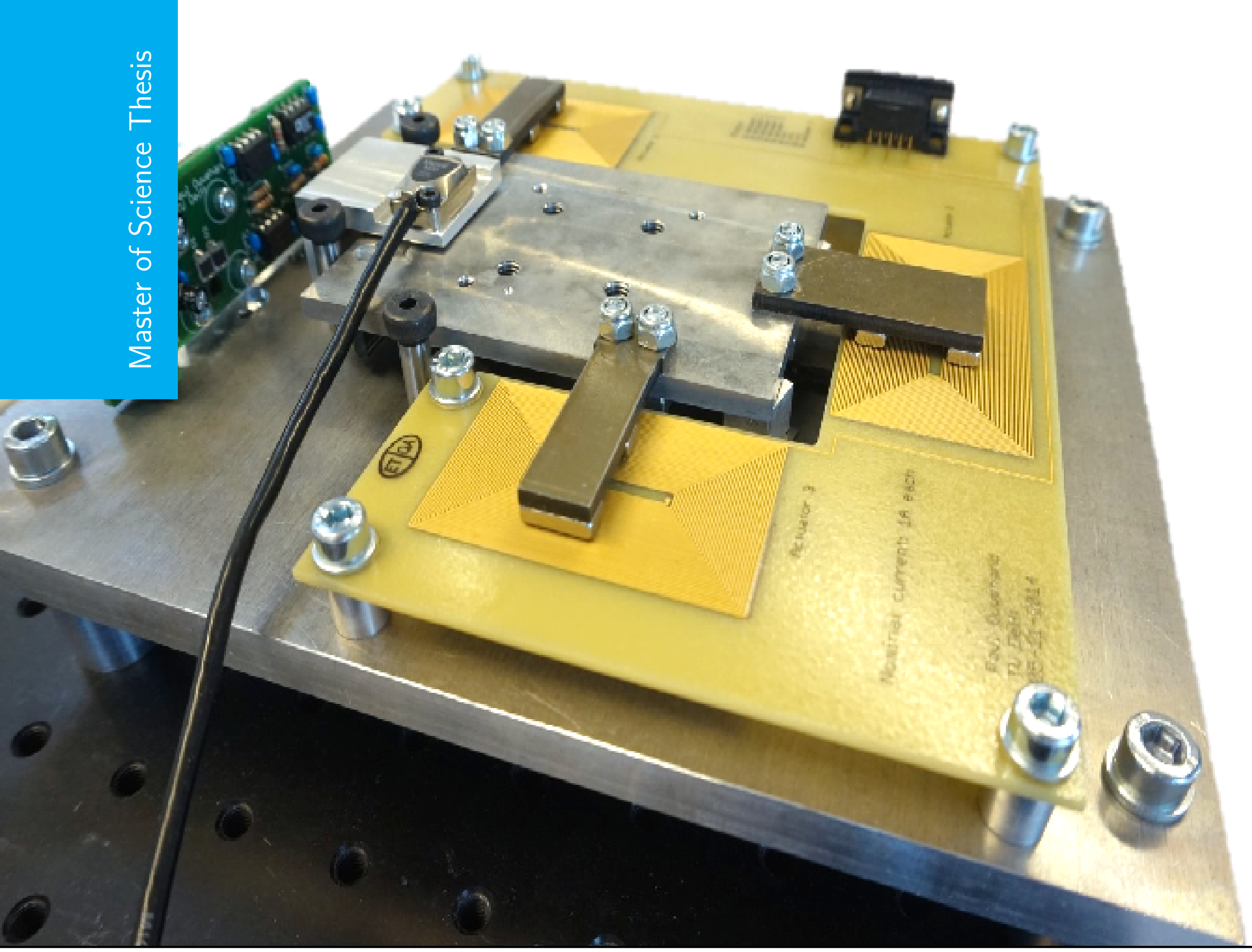

Delft University of Technology

Delft Center for Systems and Control

Model-free motion control of positioning stage

Master of Science Thesis

For the degree of Master of Science in Systems and Control at Delft University of Technology

Xiao Zhang

December 15, 2016

Faculty of Mechanical, Maritime and Materials Engineering (3mE) · Delft University of Technology

Delft University of Technology
Department of
Delft Center for Systems and Control (dcsc)

The undersigned hereby certify that they have read and recommend to the Faculty of Mechanical, Maritime and Materials Engineering (3mE) for acceptance a thesis entitled

Model-free motion control of positioning stage

by

Xiao Zhang

in partial fulfillment of the requirements for the degree of

Master of Science Systems and Control

Dated: December 15, 2016

Supervisor(s): ______________________

prof.dr.ir. J. Hellendoorn

____

Dr.ir. Hassan HosseinNia

Reader(s): ______________________

Ir.D.wilding

Abstract

Driven by the rise of market demand and development of technology, high-precision motion systems must meet the increasing accuracy requirement. Currently, High-precision positioning stage is widely used in many different application areas, such as hard disk drives, wafer steppers and electron and atomic force microscopes for nano-scale imaging. Classical PID control which occupied 95% of precision mechanical industry is no longer sufficient to satisfy the future demand for higher accuracy and performance. Therefore, the application of advanced control method on positioning stage to improve the system performance and tracking accuracy is of great importance for both academia and industry.

The challenge for the control of positioning stage lies in the strong nonlinearity such as friction or hysteresis and difficulty in modeling and identification. A novel model-free control method which has strong ability in handling nonlinearities is applied to the nano-positioning stage. This method has relatively low computational load and does not need a model. The experimental validation shows the average tracking error of model-free control reduces by 83.5% as compared with PID for the ramp tracking with maximum $50nm/s$. Both the numerical simulation and experiment results show its superiority in coping with nonlinearities and disturbance rejection. For the sake of comparison, another control method called active disturbance rejection control which has a similar structure as model-free control is also developed and applied to the positioning stage.

In terms of the drawbacks of the current model-free control method, some modifications, such as the higher order derivative estimator, the new model estimation method and nonlinear tracking differentiator, are successively applied to model-free control method to improve the tracking performance. Besides, as positioning stage often executes repetitive tasks, iterative learning control is added to compensate for repetitive error and disturbances. Moreover, a feedforward model which can predict the required force for pre-sliding motion is added to cancel the nonlinear pre-sliding friction and reduce the control effort. The numerical simulation and experiment validations illustrate, with this simple control structure, the excellent tracking accuracy and insensitivity to disturbance are ensured.

Table of Contents

List of Figures

List of Tables

Acknowledgements

Looking back at the past one year, I feel indebted to many people, in one way or another, for their encouragement and advice. Without this support, the successful completion of this thesis would surely have been impossible.

I would like to express my deepest thanks and sincere appreciation to Dr. Hassan HosseinNia and Prof.Dr.J.Hellendoorn, for kind supervision, as well as for comprehensive and creative advice during this research. It is a great honor to work under your supervision.

It is regrettable that I only had one year to work in the Mechatronic Lab in the PME department, but I will never forget this experience.

Finally, I would like to thank my parents, my family members and my friends. It would not have been possible to finish my study program in TU Delft without their love and support. This thesis is my best gift to them.

Delft, University of Technology
December 15, 2016

Xiao Zhang

Chapter 1

Introduction

1-1 Background

Driven by increasing technology development and market demand, high-precision motion systems must achieve increasing speed and accuracy requirements. Currently, high-precision positioning stage is widely used in many different application areas, including hard disk drives (HDDs) in consumer electronics, wafer steppers and scanners in nano-scale manufacturing machines, electron and atomic force microscopes for nano-scale imaging, and (nano-) printing devices. As can be seen in Figure 1-1, the stepper uses a photographic process to image nanometric circuit patterns onto a silicon wafer. For example, The wafer stage which requires the high positioning precision is an important part of lithography. As another example, the current atomic force microscopy in Figure 1-2 is able to achieve the resolution of $1nm$. Based on the different kinds of applications of positioning stage, the research for high-precision motion system has aroused extensive interests of researchers from all over the world [2].

Currently, there are many different types of positioning system. The common types are air bearing, magnetic bearing, piezo nanopositioning stage and traditional micropositioning stage. In order to achieve better positioning precision, the best positioning systems avoid friction all together, in both the drive system (motor) and in the guiding system (bearings). Frictionless bearings also avoid the bearing rumble caused by balls and rollers and provide vibration-free motion with highly constant velocity. For short travel range, piezo drives have fast response, extreme guiding precision, very long life span and can easily achieve sub-nanometer step sizes, which makes it very popular for customers. While for longer travel, air bearing and magnetic bearing positioning stage have advantages and they can avoid the impact of friction even though the cost will be higher. Positioning stage with conventional guiding cannot provide the same performance in terms of geometric precision, responsiveness and resolution, but they also have many applications due to its relatively low cost [3].

Despite the large differences in the application areas, these motion systems share a common aspect: control is essential for achieving the speed and accuracy requirements. Due to non-linear dynamics of positioning stage, the conventional PID has some limitations in obtaining

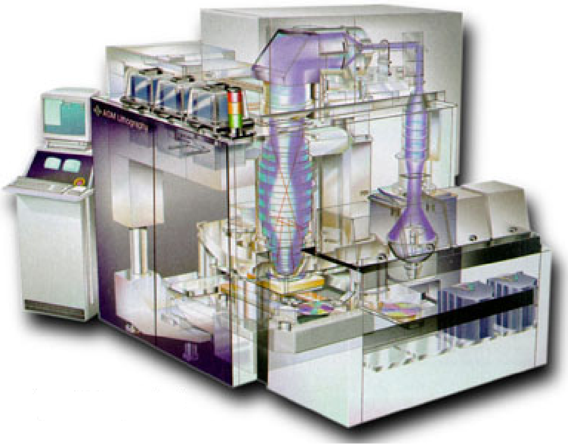

Figure 1-1: Lithography produced by ASML

Figure 1-2: atomic force microscopy

the satisfactory performance. Besides, modeling of complex and high-dimensional dynamics is another huge challenge due to the existence of possible hysteresis or friction phenomenon. These phenomenons show highly nonlinear property that is difficult for both modeling and control.

1-2 Motivation

In recent years, positioning stage has aroused intensive attraction. Since positioning stage is the base of many precision mechanical system applications, how to improve the positioning accuracy is a very popular research topic. However, there are still many challenges in the control of positioning stage, which spurs our interests for this research.

(1) Modeling: accurate modeling of positioning stage is difficult
It is well known that a good model of the system is the base of a good control for the system. An accurate model not only provides the sufficient dynamics of the system to us but helps controller to fulfill their effect as well. However, it is very difficult to obtain an accurate model for positioning stage since the existence of nonlinearities such as hysteresis and friction bring difficulties to modeling and the measured position is liable to be affected by the external disturbance. Take our experimental magnetic positioning stage as an example, the system performance is affected by friction which is highly nonlinear. Up to now, the identification for the model of positioning stage which involves friction is still a challenging research topic.

A linear model is usually used to approximate the dynamic of positioning stage in the frequency domain and nonlinear dynamics in high frequency is often neglected. Due to the difficulty in modeling and identification, optimization based method like model predictive control is difficult to be applied on the positioning stage. Based on above reasons, model-free control, which provides better performance than PID and does not need a model, will be a good alternative for realizing the good performance.

(2) Control method: low algorithm complexity and strong robustness
Although PID currently occupies more than 90% of precision motion control industry due to its relatively simple control law, it shows poor performance for the highly nonlinear system. Thus, it is necessary to use a new control method which has better ability in handling nonlinear dynamics and disturbance rejection.

The new control method should not be much complicated, the real-time processor usually has limited processing speed and computational resources. The industry prefers the simple control method which can be widely used and easily implemented rather than the complicated algorithm. Some complicated control methods are difficult to be implemented on the real setup due to the relatively high sampling frequency.

In realistic scenarios, there are all kinds of disturbances which will dramatically deteriorate the system performance, such as the vibration of bench and heat generated by PCB. Thus, the control method should have the ability to compensate or reject the external disturbances. To obtain the decent positioning accuracy, the control method should have good robustness and keep the stability of the system with less tracking errors and vibrations possible.

(3) Comparison of different control methods: in realistic scenarios with disturbances and uncertainties
Many control methods have been proposed for positioning stage in the literature. As previously mentioned, the good performance in an ideal case cannot ensure the same good performance in the realistic case. Since most the control methods are simulated in an ideal scenario so that we do not know how does the system perform with parameter uncertainties and disturbance perturbation in the real cases. Since the model of positioning stage is usually approximated by a lower order linear transfer function, it cannot accurately express the sufficient dynamic characteristic of the positioning stage due to the neglect of the system nonlinearities and disturbance.

It is not enough to evaluate the control method only from simulation result, the method should be validated in the real setup to show its advantages and disadvantages. In this thesis, several control methods will be compared in both ideal scenario and realistic scenario.

1-3 Objective and approaches

With the increasing demand for higher positioning and tracking accuracy, the classical PID control which occupied more than 90% of precision motion control industry is no longer sufficient to meet our requirement especially for a system with strong nonlinearities such as friction or hysteresis. The newly proposed model-free control, which shows strong capability in handling system nonlinearity and suppressing the noise and disturbances in simulation, will be applied to a planar positioning stage to improve the positioning accuracy.

Given the applicability and compatibility, some simple techniques namely higher-order derivative estimator, nonlinear tracking differentiator and new parameter estimation method are implemented in my thesis to improve the current drawback of model-free control. To further eliminate the system repetitive disturbance and compensate for pre-sliding friction force, an iterative learning control and a feedforward model are respectively added. These techniques have been selected because of their simple structure and design methodology. The design of the model-free control and various techniques and their simulation-based as well as experimental validation are discussed in detail in this thesis.

The ***objective*** of this research can be summarized as follows:

> "Improving the positioning and the tracking accuracy of positioning stage by introducing novel model-free control method. Based on this method, some simple but effective techniques are added to improve the current method and compensate for the friction and disturbances."

1-4 Contributions

This thesis is motivated by the challenges in the modeling and control of positioning stage discussed in Section 1-2. Therefore, the contribution of this thesis can be summarized as follows:

- A newly proposed control method, model-free control is applied to the nano-positioning stage. The simulation and experimental result show its high efficiency and robustness in the control of positioning stage.
- Comparisons of model-free control, PID and another novel control method, Active Disturbance Rejection Control (ADRC) in realistic scenarios are given.
- Some modifications aim at improving the original model-free control from different aspects have been given. The numerous simulation and experimental results show the validity and effectiveness of these new methods.
- In order to further improve the system performance, iterative learning control is combined to compensate for repetitive disturbance and achieve better tracking performance. A feedforward model which can predict the required force for pre-sliding motion is added to cancel the nonlinear pre-sliding friction and reduce the control effort. The simulation and experiment results shows, with this simple control structure, the excellent tracking accuracy and insensitivity to disturbance are ensured.

(1) Control method
Positioning stage brings many challenges: the system nonlinearity such as friction and hysteresis, external disturbances and parameter uncertainties, which set up a high requirement for the control method. Based on these requirements, a newly proposed control method, model-free control method is implemented on positioning stage. This control method can compensate well the disturbances and parameter uncertainties. It is rather simple since it does not need the accurate dynamic model. The application of model-free control method to precision mechanical system has not been seen in the existing literature. As a simple but efficient technique for nonlinear, unknown or partially known dynamics, model-free control considerably increases the tracking accuracy of the positioning stage in comparison with classical PID from the experimental validation.

(2) Comparison of control methods in realistic scenarios
In order to show the advantages and disadvantages, the other two control methods, PID and ADRC are also proposed and applied to the positioning stage. PID is the most commonly-used control method for the control of positioning stage due to its simple structure while novel ADRC which is based on an extended state observer has similar characteristics as model-free control. These three control methods are analyzed and compared with each other in the real setup to get a clear conclusion for each advantage and disadvantages. Given the particularity of nano-positioning stage, the criterions for the comparison are focused on the average tracking error and maximum tracking error, which are both very important factors for the good tracking performance. The comparison of different control methods for positioning stage are rarely presented in the existing literature.

(3) Some modifications for model-free control
Three modifications for model-free control have been implemented to improve the performance of existing method. The first exploration is to extend the general first order ultra-local model to the second order ultra-local model to test if the tracking performance will be improved. Due to the complexity of second order derivative estimation, the comparison of the second order model-free control with that of first order through the real experiment has not been seen in published literature. The second modification is to estimate the structural parameter α automatically instead of tuning it by hand, the simulation result shows, with this new method, the system works slightly better than the original method. However, more work needs to be done in future to keep the robustness of system since α may change sharply. The last modification is the introduction of tracking differentiator to model-free control for the improvement of transient process. As the experimental setup has the poor tracking performance for step signal, the addition of tracking differentiator can overcome this problem.

(4) Enhance the tracking performance by adding other methods
Given that the positioning stage often carries out the repetitive tasks and the original method cannot eliminate the repetitive disturbance, iterative learning control is combined to compensate for repetitive disturbance and achieve better tracking performance. To further enhance the tracking performance, a feedforward model which can predict the required force for pre-sliding is added to cancel the nonlinear pre-sliding friction and reduce the control effort. The simulation and experimental validations demonstrate the effectiveness of the combination of these simple algorithms and mechanisms.

1-5 Outline

This thesis is organized as follows: In Chapter 2, a short description of our experimental setup and result for system identification in the frequency domain are presented. In Chapter 3, the model-free control, active disturbance rejection control and PID are presented, model-free control is simulated and compared with the other two control methods in three different scenarios. Besides, three control methods are applied to positioning stage, the experimental result analysis and comparison are also given in this chapter. In Chapter 4, some explorations for modification of the original model-free control method are discussed, the new model-free control method will be tested in the real setup and the comparison with the current method will be illustrated. In Chapter 5, a feedforward control and iterative learning control are added to model-free control to improve system performance, iterative learning control can effectively eliminate the repetitive disturbance and feedforward model can predict required force for pre-sliding motion and reduce the control effort. The experiment result shows, with this simple control structure, the excellent tracking accuracy and insensitivity to disturbance are ensured.

Chapter 2

System description and identification

The nano-positioning stage we use in this project is supported by mechatronics lab in PME department. All the algorithm tests were implemented on this experimental setup. In this chapter, the setup including both the hardware and software is briefly introduced, which is the foundation of the subsequent controller design and performance improvement. Moreover, the frequency domain identification for the system will be shortly presented and the model will be used in the later simulation and initial tuning of PID parameter.

2-1 Nano-positioning stage

The experimental setup is a planar positioning stage. The range of positioning stage is $10mm \times 10mm$. The motion along axes are driven by three actuators. Among them, actuator 2 generates a force in X axis while the combined effort of actuator 1 and 3 is used to generate a force in the Y direction. The rotation moment is generated if the force from actuator 1 and actuator 3 is applied in opposite directions. The X and Y position will be measured by a 2D encoder system which is installed at the bottom of the mover. The stage makes use of mechanical friction between the mover and the base. This setup has high positioning resolution with relatively low scanning speed, in comparison with other conventional positioning stage. This positioning stage can be used in low-speed nano scale microscopy techniques. An advantage is that this positioning stage allows different control methods and strategies to be applied to achieve targets as displacement trajectory tracking, energy efficiency, and high dynamic performance. The architecture of system is shown in Figure 2-1

A dSPACE-1005 system equipped with DS2001 A/D and DS2102 D/A modular boards with a sampling frequency of 1 kHz is employed to implement the control strategies. The output voltage signals of the dSPACE system (0-10V) are amplified by a three-channel amplifier which generates an output current signal to drive the Lorentz actuators. Since the center of actuator 1 and actuator 3 is not installed in the same line so that a rotation moment can be generated if two forces are in opposite directions, which will lead to difficulties for the accurate motion control in the Y axis. Though we decoupled the rotation angle with

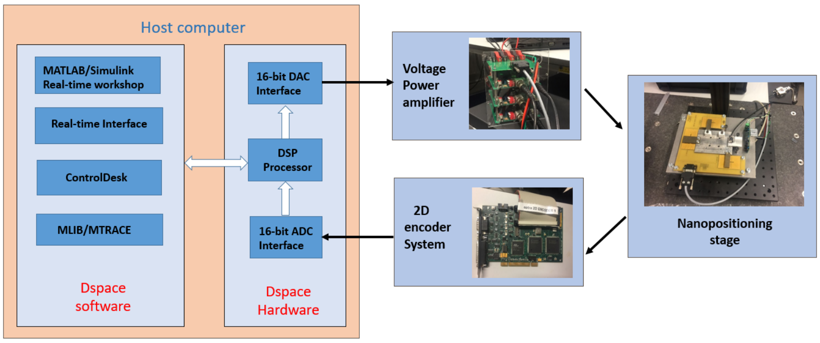

Figure 2-1: Architecture of experimental setup

motion in Y axis and try to control the rotation angle and Y-axis motion separately by two single feedback controller, due to the resolution of an optical sensor is relatively low, the completed decoupling of motion in X-axis, Y-axis and rotation angle cannot be successfully realized. Therefore, for this project, only the motion in X axis as SISO system is taken into consideration.

The main subsystems of positioning stage are:

(1) Lorentz actuator

A Lorentz actuator creates a force between the coil and the magnets. Three Lorentz actuators are being used. The actuator placement is shown in Figure 2-2. As previously mentioned, actuator 2 is used for generating forces in the x-direction and the combined effort of actuator 1 and 3 is used to generate a force in the y-direction and a probable rotation moment.

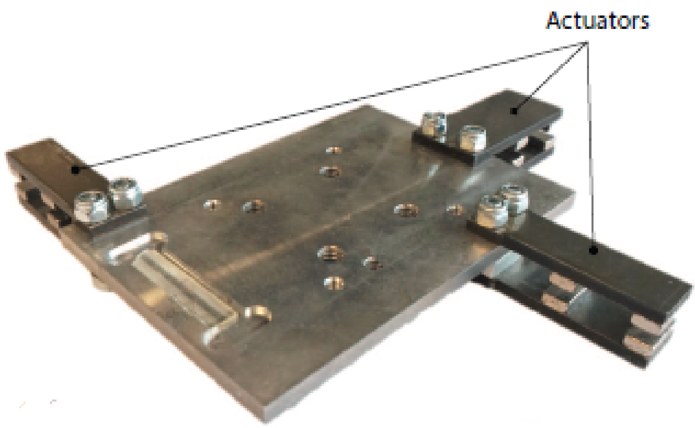

Figure 2-2: Lorentz actuator placement

Lorentz actuators have an approximately linear relation between applied current and the resulting force according to the (2-1). Besides the linearity of the Lorentz actuator, another advantage of the Lorentz actuator is that it works bidirectionally. Inverting the current direction reverses the direction of the force.

$$F = I \cdot L \times B \tag{2-1}$$

where L is the total length of the wire in the magnetic field, I is the current and B is the magnetic flux density.

(2) Amplifier

The amplifier can convert a control signal input into the electrical current output that is necessary for the actuators. Requirements for the amplifier are that it should be bidirectional and linear. By using current feedback, the output current becomes independent of the frequency dependent impedance of the actuator. The inductance of the actuator coil works as a low-pass filter, resulting in a lower output current at high frequencies. The current amplifier that is used is an operational amplifier (op-amp) where the current that passes through the load is led through a feedback resistor, resulting in a feedback voltage which is proportional to the output current. The feedback voltage is fed back into the op-amp, closing the feedback loop.

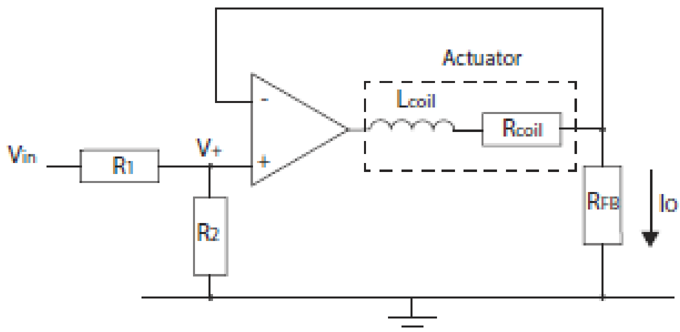

Figure 2-3: Simplified schematic of a current amplifier [1]

The relationship between the input voltage V_{in} and output current I_0 are shown in (2-2). The values of the resistors have been chosen such that the full range of the D/A converter of the control system is used. This results in a maximal current and force resolution.

$$\frac{I_0}{V_{in}} = \frac{V_+}{V_{in}}\frac{I_0}{V_+} = \frac{R_2}{R_1 + R2}\frac{1}{R_{fb}} \tag{2-2}$$

(3) 2D encoder

The position in x and y axis will be measured by 2D encoder system, The measurement system was chosen Optra Nanogrid Planar Encoder System. The Optra Nanogrid sensor system is an interferometric optical encoder system which uses the first-order diffraction of the laser reflection coming back from the grid. These types of encoders have a relatively high sensitivity and signal-to-noise ratio compared to conventional encoder systems, resulting in higher interpolation factors and hence a higher resolution. The advantage of a 2D encoder system is that it has higher resolution ($0.3nm$) compared with 1D encoder ($5nm$). Besides, 2D encoder which contains a single sensor head and a grid instead of separate scales is preferred because it can measure x and y at the same point, also minimizing errors.

(4) dSPACE platform

dSPACE is a software/ hardware platform to facilitate interfacing of Simulink models to

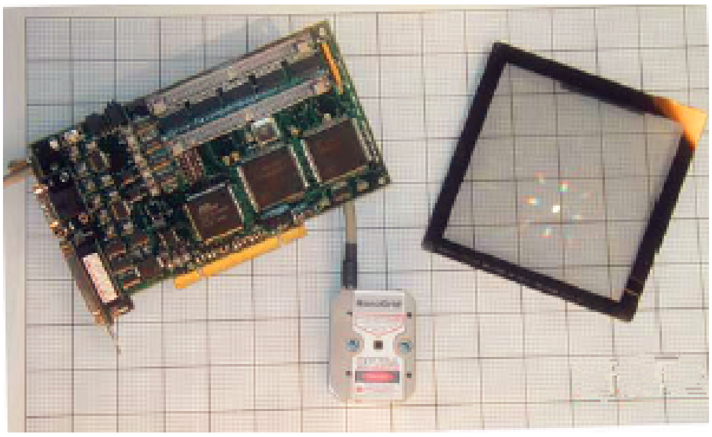

Figure 2-4: Optra 2D encoder

hardware devices in real-time. With dSPACE, hardware-in-the-loop (HIL) and rapid control prototyping (RCP) experiments can be developed quickly by using Matlab and Simulink high-level functions. The output data such as encoders measurement, general digital inputs and analog inputs can be easily read through dSPACE. The controller of each axis is implemented on a dSPACE 1005 DSP controller board, using the ControlDesk software from dSPACE to link the host computer to the drives. An additional DS2102 controller board provides the communications between the DSP controller board and the ETEL drive amplifiers using digital I/O interface. The digital I/O interface provides basic communications between the host computer and the linear drives. The more detail about the usage of dSPACE for this project and wiring diagram can be found in the appendix.

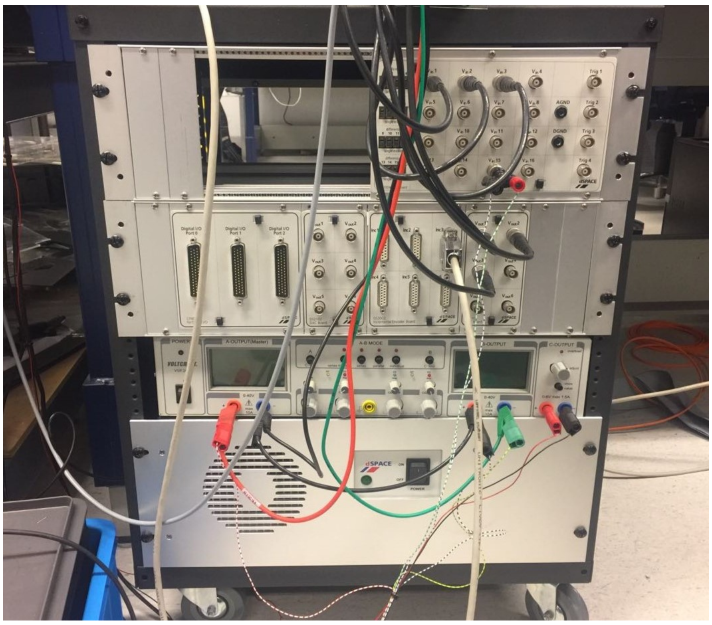

Figure 2-5: dSPACE platform

2-2 Friction in positioning system

Friction has a negative influence on the positioning resolution of positioning systems. The existence of friction can lead to three types of phenomenon: stick-slip, steady-state error and hunting[4]. The friction in positioning system can be divided into two regimes: pre-sliding regime and full-sliding regime. The pre-sliding regime is a friction regime between the stick and the slip phase. When shear forces below the stiction limit are applied on a body, elastic and plastic deformation exist, which cause a relative displacement between two contacting bodies, called the pre-sliding displacement. The pre-sliding regime is often neglected for general motion system but is very important for the precision system because it can sharply deteriorate the system tracking performance. When the shear force is above the stiction limit, full-sliding regime happens, which is considered to be a function of velocity. However, the transition between pre-sliding and full sliding is dependent on many parameters such as normal load, contact area, rate of applied force, stand-still time and contact history. This makes the exact behavior in the transition region difficult to predict and cause the difficulty in improving tracking accuracy of the system. PTFE or Teflon material is commonly applied between contacts due to its low friction coefficient. The transition between the stick and sliding phase is relatively smooth, which can reduce the stick-slip effect.

Many methods have been proposed to eliminate the friction effect. R. Leine et al. came up with a switch friction model [5] to overcome these problems. It consists of three different sets of ordinary differential equations for the description of the stick, slip and the transition. Later, many complex friction models such as the LuGre model [6] and the GMS model [7] have been successively proposed, which contain both the pre-sliding regime and full-sliding regime , but identification for the model parameter is quite complex and time-consuming. Since friction is highly nonlinear and difficult to predict and model, a simple control method will be used which can handle the system nonlinearity well and improve the system tracking performance is presented.

2-3 System identification

Although the control method does not need to have a model of the system, the identified model can be used in simulation and initial tuning of the PID controller. A linear time-invariant model of the dynamic behavior of the X axis is obtained from the frequency response function (FRF) measurements of the system. In order to measure FRFs of the system, the system is excited with a frequency sweep from 1 to 1000Hz. The output encoder measurement and the excitation signal are recorded. The sampling frequency is 1000Hz and the total duration of the measurement is 25 seconds. The FRF result for setup is shown in Figure 2-6.

From the Figure 2-6, it can be seen that the system bandwidth is quite low. The FRF contains a resonance near 450Hz and phase decrease from 0° to -180° at around 450Hz, which shows the system has two complex poles. The FRF line gradually oscillates after 700Hz due to the system nonlinearities and noise in high frequency. The system can be regarded as a second order system with a time delay.

Given the characteristics of the above FRF measurement graph, a parametric model can be fitted on the FRF measurement[8] by a second order transfer function with a time delay. The gain k, quality factor Q_1 and resonance frequency ω can be easily obtained by observation of FRF line and trial and error.

$$G(s) = \frac{X(s)}{U(s)} = \frac{k}{((\frac{s}{\omega})^2 + \frac{s}{Q\omega} + 1)} e^{-sT_d} \tag{2-3}$$

(2-3) relates the dynamic relation between input current i and table position z[m] for x axis. A summary of the estimated model parameters, k, Q, ω and T_d is given in Table 2-1.

Table 2-1: FRF identification parameters for positioning stage

parameter	k	Q	ω	T_d
value	6×10^{-7}	6	2.79×10^3	1×10^{-3}

The parametric model estimates the model as a spring line at lower frequency range and a resonance at around 450Hz. The control analysis and controller design for the positioning stage will be discussed in the next chapter.

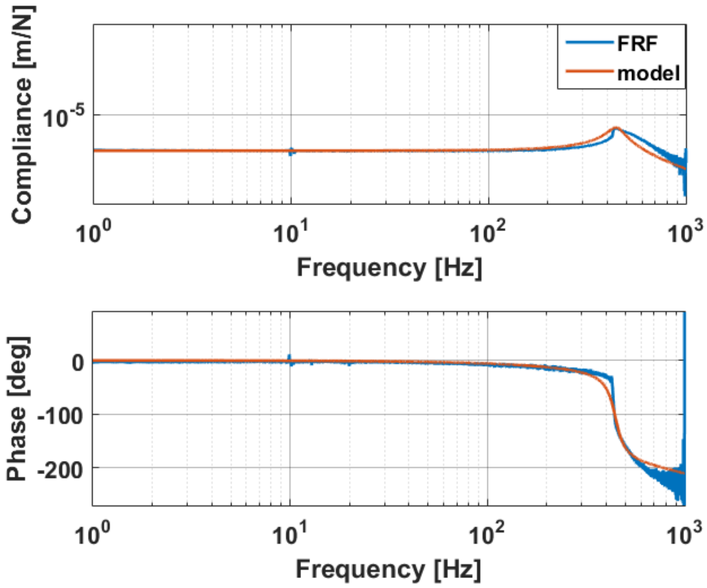

Figure 2-6: FRF measurement for system

2-4 Conclusion

This chapter discusses the constitution and operational method of the experimental setup, which is the base of subsequent controller design. As friction is highly nonlinear and it can dramatically deteriorate the system performance. Thus, the friction of positioning system is shortly discussed in this chapter. Finally, the system identification for the experimental setup is briefly illustrated. Though our model-free controller does not need a model, the identified model can be used in the basic tuning of PID parameter and simulation. The model is identified in the frequency domain. The FRF measurement of the system can be fitted by a parametric model which is a second order transfer function with a short time delay. The model is confirmed using a group of actual experimental data, which is shown in Figure 2-6.

Chapter 3

Control of positioning stage

In this chapter, we focus on design and implementation of a newly proposed nonlinear control method, which is called model-free control. To facilitate the demonstration of the advantage and necessity of model-free control, the result will be compared with classical PID control and another novel control method called active disturbance rejection control (ADRC). Initially, the simulation of these three methods for different scenarios will be presented and the result will be compared using different criterions. Then the real experimental result for these three control methods will be shown and discussed.

3-1 Model-free control design

The recently introduced model-free control provides an elegant and efficient solutions to the nonlinear system, it is a simple but efficient technique for nonlinear, unknown or partially known dynamics. While this method still keeps the merit of PID low computational load, it has the good ability to cope with system nonlinearities. So this method provides a good option for controlling nonlinear system [9].

A short review of model free control

The plant behavior can be well approximated in its operation range by a group of differential equations, which might be highly nonlinear and time-varying. The SISO system can be therefore described by the input-output equation.

$$E(t, y, \dot{y}, \ddot{y}, \cdots, y^{(l)}, u, \dot{u}, \ddot{u}, \cdots, u^{(k)}) = 0 \tag{3-1}$$

where:

- u and y are the input and output variable.

- E, which might be unkown, is assumed to be a suffciently smooth function. l is the order of derivative of output y and k is the order of derivative of input u.

The implicit function theorem for an integer n, $0 < n < l$, $\frac{\partial E}{\partial y^{(n)}} \neq 0$ can be written the following equation φ describing the input-output behavior.

$$y^{(n)} = \varphi(t, y, \dot{y}, \cdots, y^{(n-1)}, y^{(n+1)}, \cdots, y^{(l)}, u, \dot{u}, \cdots, u^{(k)}) \tag{3-2}$$

(3-2) is replaced by a numerical model, which is called ultra-local model [10] and only valid during a short time interval,

$$y^{(n)} = F + \alpha u \tag{3-3}$$

where:

- α is a non-physical constant parameter. It is obtained by trials and errors that F and αu are of the same magnitude.
- $y^{(n)}$ is the derivative of order of y. The integer n is selected by the practitioner.

The numerical value of F, which contains the whole 'structural information', both system dynamics as well as possible disturbances, are determined thanks to the knowledge of u, α and estimation of the derivative $y^{(n)}$. The value F can be estimated by $\hat{F}$ as in (3-4):

$$\hat{F} = \hat{y}^{(n)} - \alpha u \tag{3-4}$$

A model free controller is defined as:

$$u = \frac{1}{\alpha}(y_r^{(n)} - \hat{F}) + \Lambda(e) \tag{3-5}$$

where:

- y_r is a reference trajectory
- $e = y_r - y$ is the tracking error. $\Lambda(e)$ is a function which makes the closed loop error dynamics $e^{(n)} = \Lambda(e)$ asymptotically stable. $\Lambda(e) = K_{n-1}e^{(n-1)} + K_{n-2}e^{(n-2)} + \cdots + K_1\dot{e} + K_0 e$, where $K_i, i = 0, \cdots, n-1$ are tuning gains.

Combining (3-4) and (3-5) yields the functional equation:

$$e^{(n)} + \Lambda(e) = 0 \tag{3-6}$$

Λ should be selected such that a perfect tracking is asymptotically ensured[11], i.e.

$$\lim_{t\to\infty} e(t) = 0 \tag{3-7}$$

Intelligent PID

Many control methods can be used as a feedback controller to connect with model free non-linearity compensator, however, PID is the most simple one among them and it is called intelligent PID by [10]. If PID is selected, the desired closed loop behavior can be obtained thanks to a model-free controller as follows (assumed order of derivative $n = 1$):

$$u(t) = \frac{-\hat{F}(t) + \dot{y}_r(t)}{\alpha} + K_p e(t) + K_i \int e(t) + K_d \dot{e}(t) \tag{3-8}$$

where K_p, K_i and K_d are tuning gains for model-free controller, the tuning of K_p, K_i and K_d is straightforward for model-free controller. It boils down to the stability of a linear differential equation of order three, with constant coefficients.

Since the computer implementation is in discrete time, the ultra-local model can be rewritten into discrete time form as:

$$\hat{F}(k) = \hat{\dot{y}}(k) - \alpha u(k-1) \tag{3-9}$$

The control law of model free control can be written as:

$$u(k) = \underbrace{-\frac{\hat{F}(k)}{\alpha} + \frac{\dot{y}_r(k)}{\alpha}}_{nonlinear\ cancellation} + \underbrace{\Lambda(e)}_{close\ loop\ tracking} \tag{3-10}$$

where $\Lambda(e)$ is the transfer function of the PID controller The stability condition is similar to the previously mentioned continuous system (3-6) and (3-7). Given that the above error equation is linear, our task is to tune the parameters K_p and K_i and K_d to obtain a good tracking of y_r. It should be noted that the structural of model free control can be regarded as a feedforward controller plus a feedback PID control. Feedforward control can cancel the system nonlinearity as well as the disturbances, closed-loop feedback control will eliminate the error and realize the good tracking. The structure for model-free control are shown in Figure 3-1

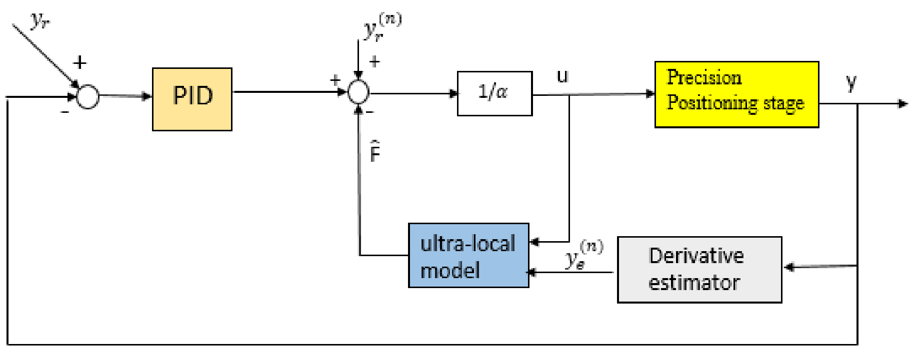

Figure 3-1: Block diagram of the model free control for positioning stage

Derivatives of noisy signals

As can be seen in (3-9), it is obvious that the accurate estimation of F lies in the estimation of $\hat{y}$, now the problem can be boiled down to accurate estimate the derivative of output in real time [12], J. Zehetner et al. has introduced a fast and robust derivative estimation method [13] which can be used to estimate the parameter for previously mentioned model-free controller.

This novel method is based on Laurent Schwarz calculus of distributions and operational calculus respectively. This method consists in designing FIR filters resolving a classical polynomial approximation of the signal. The polynomial approximation is obtained by algebraic manipulation of signals in the operational domain. We consider a signal y that is available through a measurement y_m corrupted by some additive noise ω, i.e. $y_m = y+\omega$. The objective is to estimate time derivatives of signal $y(t)$, up to a finite order, from its measurement y_m. Consider a real-valued, analytic function of time, $y(t)$ which for time instants $t > 0$ can be approximated by its Taylor-series expansion.

$$y(t) \approx y_N(t) = \sum_{t=0}^{N} \frac{y^{(i)}(0)}{i!} t^i \tag{3-11}$$

of order N. We transform the equation from time domain to operational domain and obtain:

$$Y_N(s) = \frac{y(0)}{s} + \frac{\dot{y}(0)}{s^2} + \cdots + \frac{y^{(N)}(0)}{s^{N+1}} \tag{3-12}$$

We can equivalently modify the above equation by a left multiplication by an appropriate operator which helps isolate the *j-th* coefficient $a_j = y^{(j)}(0), j = 0, 1, 2, 3, ..., N$. Through complex operational calculus deduction and transformation, finally we can derive (3-13) (ν can be chosed any number larger than 0). Interested reader might refer to [13] for a complete presentation.

$$a_j = \int_o^t \Pi_{jN\nu}(t,\tau) y_N(\tau) d\tau \tag{3-13}$$

with

$$\begin{aligned} \Pi_{jN\nu}(t,\tau) = \frac{(N+j+\nu+1)!(N+1)!(-1)^j}{t^{N+j+\nu+1}} \sum_{\kappa_1=0}^{N-j} \sum_{\kappa_2=0}^{j} \\ \frac{(t-\tau)^{\nu+\kappa_1+\kappa_2}(-\tau)^{N-\kappa_1-\kappa_2}}{\kappa_1!\kappa_2!(N-j-\kappa_1)!(j-\kappa_2)!(N-\kappa_1-\kappa_2)!(\nu+\kappa_1+\kappa_2)!(N-\kappa_1+1)} \end{aligned} \tag{3-14}$$

In course of time, the Taylor-series expansion (3-11) becomes inaccurate because it holds only in the vicinity of $t = 0$. On the contrary, what we interested in is the derivative estimates at a time instant $t \gg 0$. Therefore, the above formulas have to be adapted through the expansion y at the time instant of interest. Finally, we obtain:

$$y^{(j)}(t) = (-1)^j \int_0^T \Pi_{jN\nu}(t,\tau) y(t-\tau) d\tau \tag{3-15}$$

Note that the integral operation plays the role of a low-pass filter and reduces the noise that corrupts the signal y_m. The choice of T and N results in a trade-off: the larger is T, the smaller is the effect of the noise (the larger is T the better is integrals low pass filtering) and the larger is the error due to truncation.The larger is N, the smaller is the error due to truncation and the larger is the error due to noise.

With $N = 1, j = 1, \nu = 0$, we can obtain:

$$\hat{y} = -\frac{3!}{T^3}\int_0^T (T - 2t)y(t)dt \tag{3-16}$$

Since the derivative estimation will be realized by the FIR filter, the value of the signal is approximated by a trapezoidal numerical integration. For discrete time values, we obain the approximation

$$y_k^j \approx (-1)^j \frac{T_s}{2}\sum_{i=1}^{M}(\Pi_{i-1}y_{k-i+1} + \Pi_i y_{k-i}) \tag{3-17}$$

where $t_{k-i} = (k-i)T_s$ and $t_i = iT_s$, $y_{k-i} = y(t_{k-i})$ and $\Pi_i = \Pi_{jN\nu}(T, t_i)$. T_s is the sample time and M denotes the number of summation steps, it holds $M = T/T_s$.

3-2 Active disturbance rejection control

Recently, another novel control method which has a good ability to handle complex system (nonlinear,time-varying, etc) has aroused broad attention. This method does not need a model and has similarities in some aspects with the previously mentioned model-free control, thus will be discussed in this section.

The ADRC method assumes that a resultant of the modeling uncertainty and external disturbances can be considered as one of the states of the system [14]. An estimation of state provided by a state observer can be further used in the control signal to compensate for the real perturbation in the plant. The general ADRC consist of three components [15]: the nonlinear tracking differentiator (TD), the nonlinear state error feedback (NLSEF) and the extended state observer (ESO). ESO is the core component of ADRC, which can estimate the system's state and obtain the uncertain disturbances arising in the nanopositioning system. Therefore, a feedforward control will be generated to compensate the disturbances before they can affect the system positioning performance, which has similarity with the previously mentioned model-free control. The schematic diagram of the ADRC is shown in Figure 3-2.

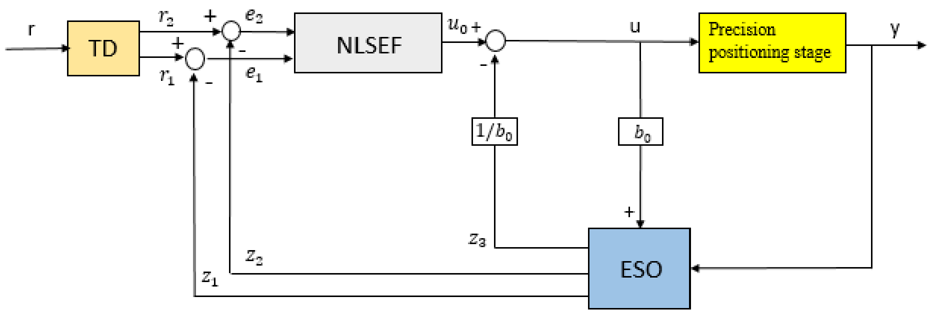

Figure 3-2: Block diagram of the ADRC for positioning stage

TD design

Nonlinear TD is used to arrange the desirable transient dynamical procedure. The output signal can keep the desired speed and has less overshoot, which can be realized by adjusting the parameter δ and h. Besides, TD has the ability to filter the noise signals of input so that the output differential signal will be less affected by the noisy input. The discrete forms of the reference signals r_1 and r_2 of the presented TD in the feedforward path are expressed as follows:

$$\begin{cases} r_1(k+1) = r_1(k) + hr_2(k) \\ r_2(k+1) = r_2(k) + hfhan(r_1(k) - r(k), r_2(k), \delta, h) \end{cases} \tag{3-18}$$

where h is the sampling step and δ is a velocity factor which will determine the transition. The function $hfhan(r_1(k) - r(k), r_2(k), \delta, h)$ can be expressed as follows:

$$fhan(x_1, x_2, \delta, h) = -\begin{cases} \delta sign(a), & |a| > d \\ \delta \dfrac{a}{d}, & |a| \leq d \end{cases} \tag{3-19}$$

where a and d will be determined by

$$a = -\begin{cases} x_2 + \dfrac{(a_0 - d)}{2} sign(y) & |y| > d_0 \\ x_2 + \dfrac{y}{h} & |y| \leq d_0 \end{cases} \tag{3-20}$$

with

$$\begin{cases} d = \delta h \\ d_0 = hd \\ y = x_1 + hx_2 \\ a_0 = \sqrt{d^2 + 8\delta |y|} \end{cases} \tag{3-21}$$

Therefore, for any bounded integrable function $r(k)$, the formula expressed by (3-18) can be utilized as a high-performance tracking differentiator,i.e. $r_1(k) \to r(k)$, $r_2(k) \to \dot{r}(k)$ [16].

ESO design

For nano-positioning stage, the plant model is hard to be identified due to factors such as mechanical vibration, friction, creep, thermal drift, sensor noise and temperature variation. The ESO observer, which takes all nonlinearity factors as the total disturbance, will estimate and reject the unknown total disturbances before the disturbances degrade the system performance[17]. An $(n+1)$th-order ESO for the system can be expressed as (3-22):

$$\begin{cases} z_1(k+1) = z_1(k) + h(z_2(k) - \beta_1 \varepsilon_0) \\ z_2(k+1) = z_2(k) + h(z_3(k) - \beta_2 fal(\varepsilon_0, \alpha_1, \delta_1)) \\ \cdots \\ z_n(k+1) = z_n(k) + h(z_{n+1}(k) - \beta_n fal(\varepsilon_0, \alpha_1, \delta_1) + b_0 u(k)) \\ z_{n+1}(k+1) = z_{n+1}(k) - h\beta_{n+1} fal(\varepsilon_0, \alpha_2, \delta_1) \end{cases} \tag{3-22}$$

where $\varepsilon_0 = z_1(k) - y(k)$; z_1 and z_2,$\cdots$,z_n are the estimated system's states, i,e., $z_1 \to y_1$, $z_2 \to y_2$,$\cdots$,$z_n \to y_n$, z_{n+1} is the estimated unknown disturbances; and α_i $(i = 1, 2, \cdots, n+1)$

and δ_1 are the design parameters to be determined. The function $fal(\varepsilon, \alpha, \delta)$ is defined as follows:

$$fal(\varepsilon, \alpha, \delta) = \begin{cases} |\varepsilon|^{\alpha} sign(\varepsilon) & |\varepsilon| > \delta \\ \dfrac{\varepsilon}{\delta^{1-\alpha}} & |\varepsilon| \leq \delta \end{cases} \tag{3-23}$$

The order of ESO can be selected by practioner. In most cases, the order of ESO is selected to be 1 or 2. For this project, we use second order ESO. The output of the ESO provides the important dynamic information $z_3(t)$, which will be compensated by the control signal.

NLSEF design

Similar to the previously-mentioned model free control, ADRC can be also regarded as feedback control plus a feedforward control, the feedforward term is derived from the estimation of observer, the closed-loop feedback control will eliminate the error and achieve good tracking. Many control method can be used to connect with ESO, the common-used methods are PD controller and NLSEF method. Since NLSEF is easy to be implemented and the performance is better than classical PD controller, NLSEF is chosen as the control method.

Once the differential signals and the estimated states are obtained, the essential elements of the traditional PD controller can be replaced by

$$\begin{cases} e_1(k) = r_1(k) - z_1(k) \\ e_2(k) = r_2(k) - z_2(k) \end{cases} \tag{3-24}$$

Thus, the control method can be generated by using the aforementioned two components:

$$u_0 = k_p fal(e_1, \alpha_{01}, \delta_0) + k_d fal(e_2, \alpha_{02}, \delta_0) \tag{3-25}$$

where the parameters k_p, k_d, α_{01}, α_{02} and δ_0 are to be determined.

The total control signal of the ADRC will be derived by

$$u = u_0 - \frac{z_3(k)}{b_0} \tag{3-26}$$

3-3 PID control design

PID is the most common-used control method for precision motion system since it is easy to be implemented in real setup. The control law of classical PID is as follows:

$$u_x = k_p e_t + k_i \int_0^t e(\tau) d\tau + k_d \frac{d}{dt} e(t) \tag{3-27}$$

The system performance lies in the tuning of three PID parameters, namely: k_p, k_i and k_d. In order to tune the parameters in frequency domain, we obtain the FRF measurement for open loop transfer function $L(s)$ and closed loop transfer function $T(s)$ by adding a sine frequency sweep signal from 1 to $1000Hz$ as the input signal. The PID transfer function $C(s)$ is utilized to choose the desired shape for $L(s)$. The system bandwidth has been increased to $30Hz$, the open loop transfer function $L(s)$ and closed loop transfer function $T(s)$ are shown in Figure 3-3 and Figure 3-4, the parameters for PID are: $k_p = 3.22 \times 10^6$, $k_I = 1 \times 10^6$, $k_d = 2.07 \times 10^4$

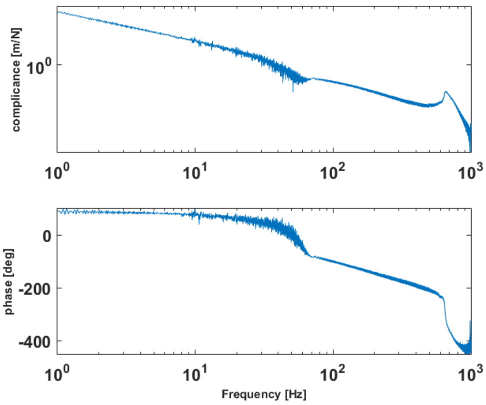

Figure 3-3: Open loop response $L(s)$

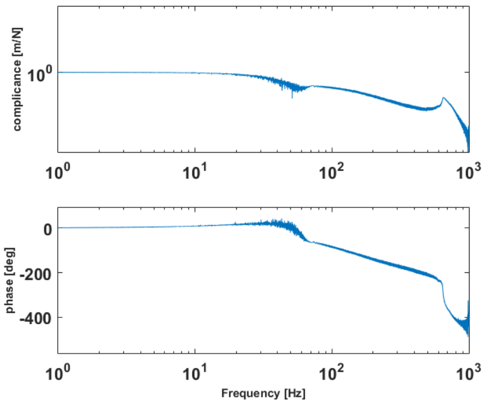

Figure 3-4: Closed loop response $T(s)$

3-4 Simulation for robustness analysis

In this section, model-free control, ADRC and PID will be simulated for three different scenarios to test the robustness of controller. The result will be compared in terms of different criterions which are proposed at the beginning and a clear conclusion will be drawn from the simulation result.

3-4-1 Criterion for comparing different control method

In order to facilitate the comparison of above mentioned three control methods, we set several criterions which fully consider the characteristic of the nano-positioning stage. For the application of nano-positioning stage, tracking error is the most important factor we take into consideration. The maximum absolute tracking error and average tracking error are both very crucial criteria for evaluating the tracking error. Except for the tracking error, Robustness of the control method is another factor which we will put emphasis on. As previously mentioned, the performance of the positioning stage will be affected by a variety of external disturbances such as mechanical vibration, thermal drift and temperature variation. A good controller should have the ability to reject disturbances and keep the system stable with the noise and disturbance perturbation. Thus, we add robustness criterias to the list to make it sufficient and comprehensive for evaluating the system performance. The list is shown as follows:

- Maximum absolute tracking error: ϵ_{max}.
- Average of the absolute tracking error $\epsilon_{avg} = \frac{1}{N}\sum_{i=1}^{N}\epsilon_i$.
- Robustness to model uncertainties: the sum of the square of the tracking errors (ISE) under parameter uncertainty $\int_t \epsilon_i^2$
- Robustness to external disturbances: the sum of the square of the tracking errors (ISE) under external disturbance $\int_t \epsilon_i^2$.
- Adjusting time to disturbances: the time needed to return to the stable state t.

3-4-2 Disturbances of positioning stage and correponding simulation strategy

In real applications, circumstances can be rather turbulent, which results in a totally different effect on positioning stage to the scenario without disturbance. In order to make the simulation close to the real scenario, the different disturbance effect is researched and simulated. Control methods are tested for different disturbances such as the mechanical vibration, actuator and sensor noise, model parameter uncertainty.

Model parameter uncertainties

Model parameter uncertainty analysis is dedicated to test the tolerance of control systems to modeling errors. Some dynamics are lost in our model when we fit a linear model to the measured experimental data in frequency domain. Except for the modeling error, for the application of positioning stage, thermal effect is the main disturbance which will dramatically degrade system performance. The heat generated by PCB will lead to the variation of magnetic flux density. The thermal effect can be regarded as model parameter uncertainty. The rise of temperature will gradually increase the difference between the real dynamics and the model. The thermal effect on positioning stage will be simulated as model parameter uncertainty case and the comparison for different control methods will be presented in this section.

Assumed the plant model is $G_p(s)$, its nominal model which is introduced in Section 2-3 is $G_n(s)$. All the dynamic uncertainty lump into the multiplicative uncertainty which is utilized to describe our uncertainty set. The expressions for multiplicative uncertainty is shown as:

$$G_p(s) = G_n(s)(1 + \Delta(s)) \tag{3-28}$$

By observing the measured experimental data and the output of model in the frequency domain (Figure 2-6), the Δ_{max} can be easily calculated, which is: $\Delta_{max} = 0.027$. Since the thermal effect is difficult to be expressed mathematically and it will gradually increase while the setup is running, The model is replaced by a new plant model which equals to the identified model times the maximum uncertainty $\Delta = 0.05$ at 150 seconds to test the robustness of controller under the extreme situation. As for the real experiment, model variation is a gradual change process. For the sake of simplicity, we consider it as a sudden change to test the robustness of controller under the worst situation.

To test and compare the performance of the controller under model variation, the identified model (Table 2-1) is used for simulation from 0 to 150 seconds and replaced by the above mentioned model from 150s. The performance of different control methods will be compared in terms of the previously mentioned criterion.

External disturbance

This scenario is dedicated to test the stability of control systems while encountering environment disturbance. Positioning stage is easy to be affected by external disturbances while it is operating, any tiny external perturbation can affect the system performance. Some of sudden external disturbances are so tiny that we cannot even feel it, but it can result in the larger tracking error and the degradation of the system performance. Mechanical vibration caused by the shake of experimental bench is the main external disturbance for the positioning stage. Since mechanical vibration usually occurs in a sudden and the dynamics is hard to be expressed mathematically, we use an additive square wave force signal to simulate the effect of external disturbance.

A square wave force signal with magnitude $0.0015N$ for the time range from 139s to 140s is added to system. The performance of different control methods will be compared and analysed.

Actuator and sensor noise

This scenario is dedicated to test the tolerance of control systems to noises of the system states. Generally, actuator and sensor noise cannot be avoided for any system. Due to the high requirement for the positioning accuracy of positioning stage, the system performance can be severely affected by actuator and sensor noise. The control method should have the ability to suppress the actuator and sensor noise and keep good tracking performance.

Gaussian white noise with $N(0, 0.01^2)$ is added to the measurement to represent the actuator and sensor noise, the result will be compared for three different control methods.

Three scenarios for simulation

Since the model identified is a linear model and nonlinear dynamics such as friction have been neglected, it is unnecessary to compare the ideal scenario which has no noise and disturbance perturbation. The system performance will not have a big difference for three control methods in the ideal scenario. Our main interest is which control method has better ability to suppress the noise and keep the system stable when the noise and disturbance are added. Without losing generality, three scenarios are proposed for the simulation and can be concluded as follows:

- **Scenario 1**: Sensor and actuator noise is added only;
- **Scenario 2**: Sensor and actuator noise is added and the plant model is changed from 150s;
- **Scenario 3**: Sensor and actuator noise is added and a sharp mechanical vibration is added from $139s$ to $140s$.

3-4-3 Simulation result

Table 3-1: The comparisons of different control conthods in scenario 1

scenario 1	MFC	ADRC	PID
Maximum absolute tracking error: ϵ_{max} $[nm]$	8.47	23.81	7.78
Average of the absolute tracking error: ϵ_{avg} $[nm]$	0.57	0.21	1.15

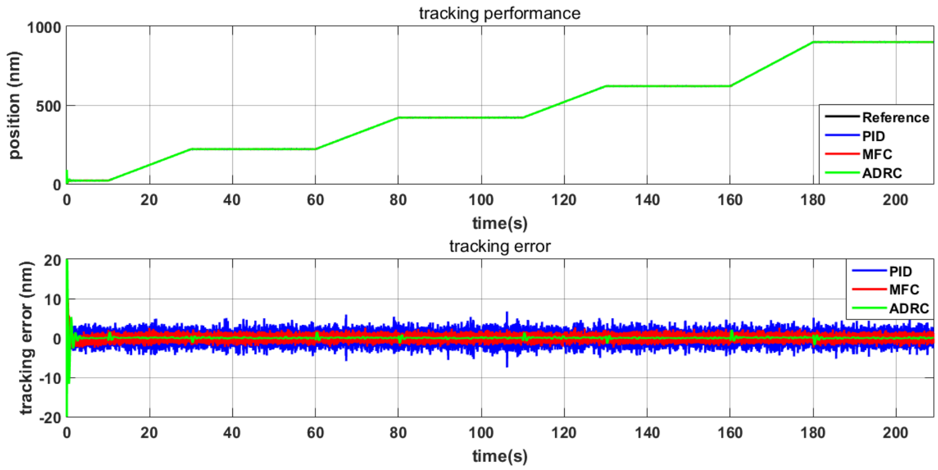

Figure 3-5: Control methods comparison for scenario 1

As can be seen in Figure 3-4 and Table 3-1, ADRC has the least average tracking error (0.21 nm) while PID has the largest tracking error (1.15 nm) with sensor noise perturbation. For ADRC, ESO provides the estimation of noise by the extended state z_3 and eliminates the estimated noise before it can affect system positioning performance. Thus, ADRC has the best noise reduction ability among three controllers. The MFC also has decent noise reduction and the ability mainly comes from the derivative estimator which is realized by the form of the FIR filter. The FIR filter can be regarded as a low pass filter and reduces the noise. However, due to the limit of estimated horizon T, it is only valid for the noise with the frequency above a specific value. Thus, the noise reduction ability for MFC is slightly weaker than ADRC. In terms of maximum absolute tracking error, MFC and ADRC is larger than PID, which is mainly caused by the larger overshoot in the initial transient stage. ADRC has the similar structure as MFC and the input gains are tuned by the practitioner, which can result in the poor performance in the initial transition. This phenomenon can also be found in other applications [18]. We can let the control algorithm work for a while before the desired manipulation start. Except for the error in the initial transition, the tracking error of MFC and ADRC are much less than PID.

Table 3-2: The comparisons of different control conthods for scenario 2

scenario 2	MFC	ADRC	PID
Maximum absolute tracking error: ϵ_{max} $[nm]$	46.54	96.50	88.72
Average of the absolute tracking error: ϵ_{avg} $[nm]$	0.69	0.76	1.29
Maximum of tracking error (model variation from $150s$) $[nm]$	46.54	46.38	88.72
Integral Squared Error (model variation 150s-152s)	19442	19016	72817
Adjusting time to model uncertainty t $[s]$:	1.65	1.73	1.97

Due to some unknown factors such as thermal effect and flatness of the contact surface, the plant model changes continuously, which sets a high requirement for the robustness of our control method. In scenario 2, we want to test the performance of different control methods under the model variation and parameter uncertainties. As can be seen in Figure 3-6 and Table 3-2, when the model is changed at 150s, the maximum of tracking error and error

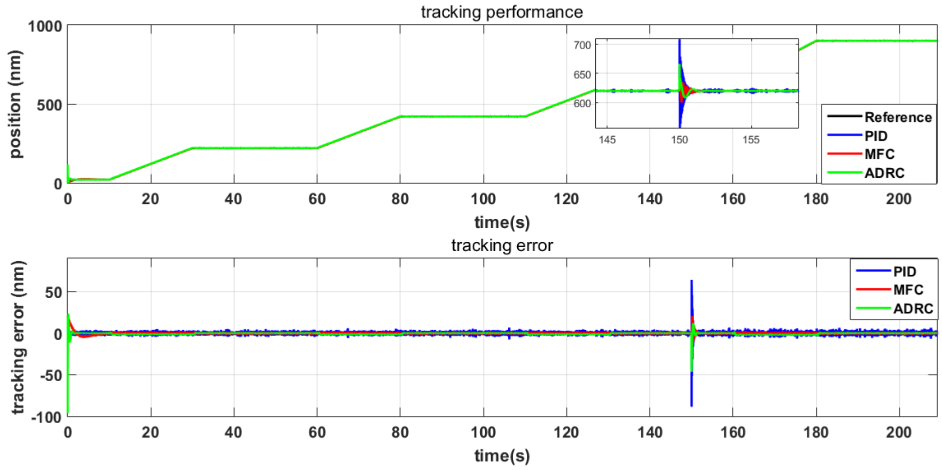

Figure 3-6: Control methods comparison for scenario 2

variance for MFC and ADRC are much less than PID, which shows MFC and ADRC have better ability to cope with the model variation and parameter uncertainty. This is a crucial advantage for the application of positioning stage. The value of maximum tracking error, error variance and adjusting time for MFC and ADRC are similar, which demonstrates that the two methods have similar ability in handling system uncertainty. As previously mentioned, MFC and ADRC have the similar structure and they both can be regarded as a feedback control with a feedforward compensator, only the realization forms are different. However, since more parameters of ADRC need to be tuned by the practitioner and the tuning process is quite tricky, the performance of ADRC heavily relies on the parameter tuning.

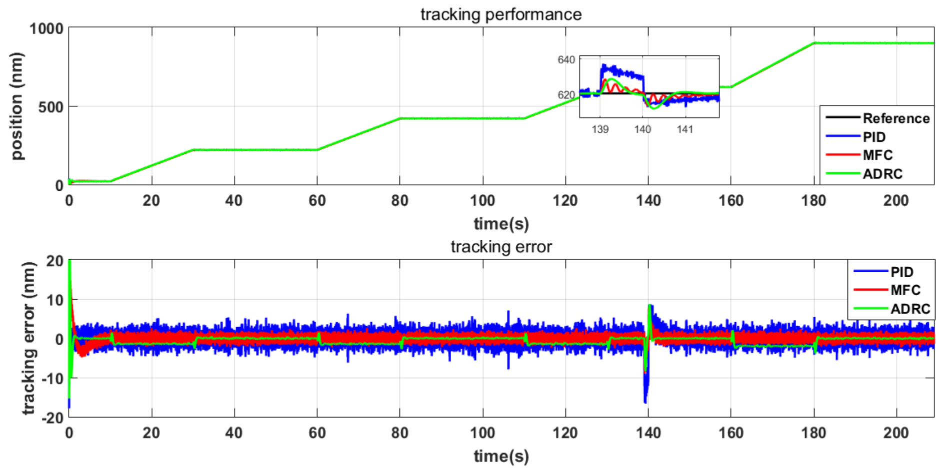

Figure 3-7: Control methods comparison for scenario 3

As the positioning stage is very sensitive to the environment change and external disturbance. For the scenario 3, we want to compare the performance of different control methods when a sudden external disturbance is added from 139s to 140s. From Figure 3-7 and Table 3-3, the maximum tracking error, error variance and adjusting time for MFC and ADRC are much less than PID, which corresponds to the fact that the MFC and ADRC have better ability in disturbance rejection. Compared with ADRC, MFC has less error variance while

Table 3-3: The comparisons of different control conthods for scenario 3

scenario 3	MFC	ADRC	PID
Maximum absolute tracking error: ϵ_{max} $[nm]$	20.74	23.09	20.20
Average of the absolute tracking error: ϵ_{avg} $[nm]$	0.63	0.75	1.27
Maximum of tracking error (139s-144s) $[nm]$	8.99	8.73	16.65
Integral Squared Error (external disturbance 139s-144s)	4662	8929	37294
Adjusting time to external disturbance: t $[s]$:	3.4s	2.5s	4.6s

adjusting time is a little bit longer. MFC responds quickly to the external disturbance due to the real time computation of the parameter $\hat{F}$ while for ADRC, the unexpected disturbance is considered in an extended state z_3 and estimated by ESO in real-time. Through the simulation, we can conclude that ADRC has the best noise rejection ability among the three control methods. Compared with PID, both ADRC and MFC have stronger ability to handle the model and parameter uncertainty and reject the external disturbance, which is appealing to us.

3-5 Experimental validations and result

Experimental validation of PID, MFC and ADRC is performed on the previously mentioned experimental positioning stage. The reference is again a line signal, which consists of four ramp signal. The slope of each ramp signal is respectively $10nm/s$, $10nm/s$, $10nm/s$ and $15nm/s$. The purpose of utilizing this ramp signal is that we want to gradually increase the tracking velocity to reduce the possibility of losing stability in the initial stage. The measured position and position tracking errors are recorded. The experimental result for PID, MFC and ADRC for maximum $15nm/s$ are respectively shown in Figure 3-8, Figure 3-9 and Figure 3-10. Table 3-4 lists a summary of the tracking experimental results for three control methods.

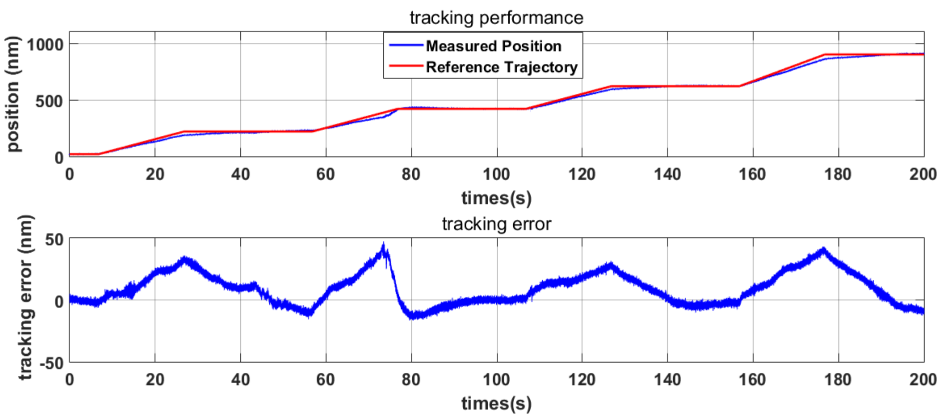

Figure 3-8: Measured position and tracking error for PID for maximum velocity 15nm/s

From experimental result, ADRC yields the least average for tracking error and maximum of absolute tracking error. It achieves respectively 81% and 73.6% reduction for the maximum

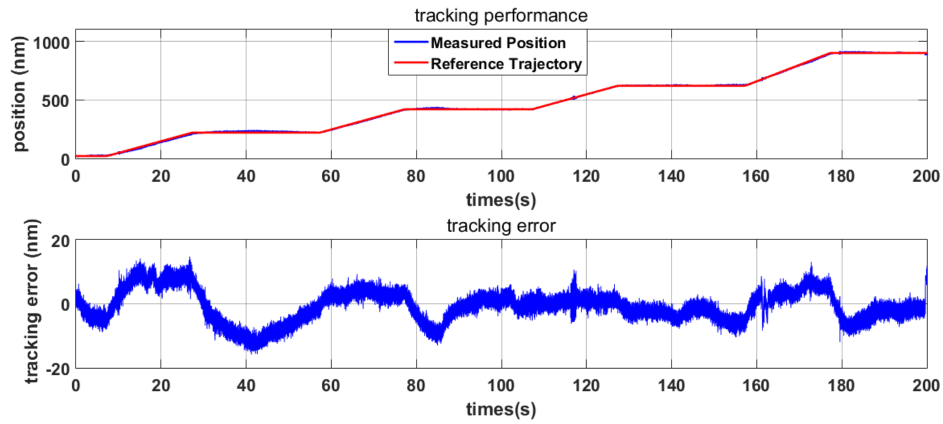

Figure 3-9: Measured position and tracking error for MFC for maximum velocity 15nm/s

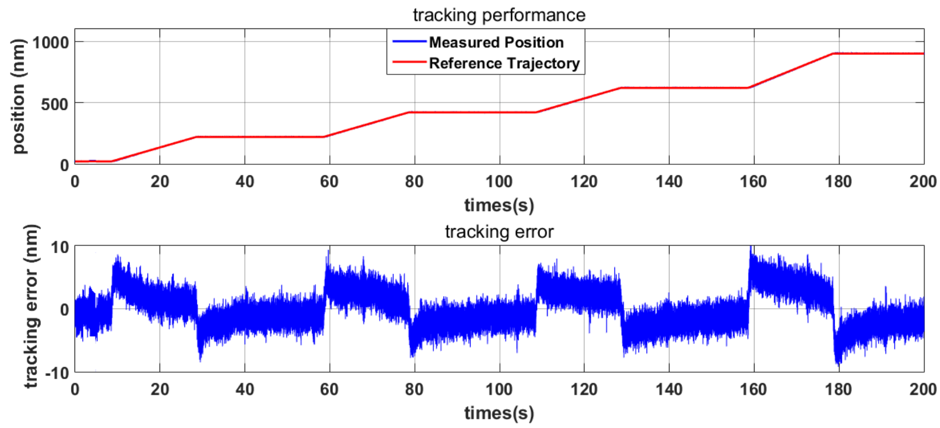

Figure 3-10: Measured position and tracking error for ADRC for maximum velocity 15nm/s

Table 3-4: Experimental result for reference ramp tracking with maximum 15nm/s uisng PID, Model-free control, ADRC

Parameter	PID	MFC	ADRC
Maximum of tracking error: ϵ_{max} $[nm]$	48	14	9
Average of the tracking error: ϵ_{avg} $[nm]$	12.4	3.9	3.3
Maximum of tracking error (after $v = 15nm/s$) $[nm]$:	48	10	9
Average of tracking error (after $v = 15nm/s$) $[nm]$:	17.7	3.9	3.5

of tracking error and the average of tracking error with ADRC in comparison with PID. MFC also yields decent tracking performance with average of tracking error $3.93nm$ which is similar to that of ADRC. The result when the tracking velocity reaches $15nm/s$ is taken separately for the calculation and analysis. As can be seen in Table 3-4, the average of tracking error for PID dramatically increases when the tracking velocity increases while it is steady for MFC and ADRC with the increase of velocity. The results illustrate that the utilization of MFC and ADRC can significantly improve the tracking performance of positioning stage in comparison with PID.

Next, the new ramp signal with higher tracking velocity is used to test the performance of three control methods. The reference consists of three ramp signals and each slope is respectively $10nm/s$, $30nm/s$ and $50nm/s$. The measured position and position tracking errors are recorded. These results are shown in Figure 3-11,Figure 3-12 and Figure 3-13. A summary of the tracking performance of different control methods with maximum $50nm/s$ will be listed in Table 3-5.

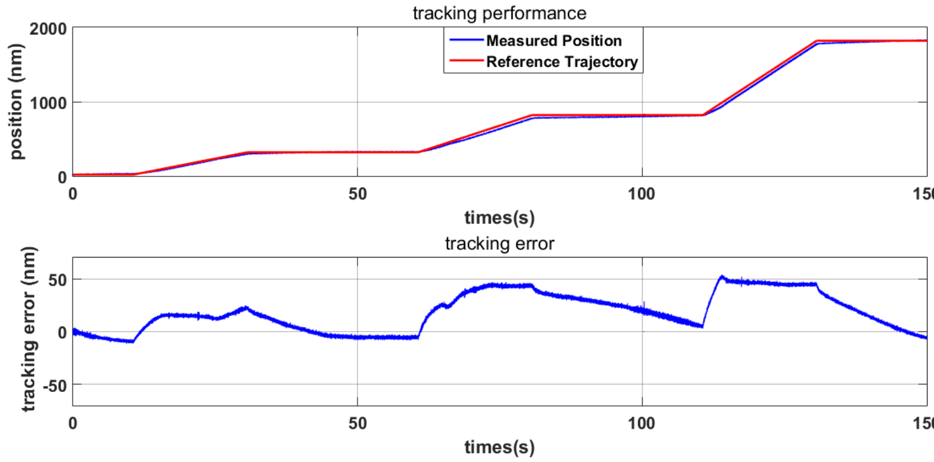

Figure 3-11: Measured position and tracking error for PID for maximum velocity 50nm/s

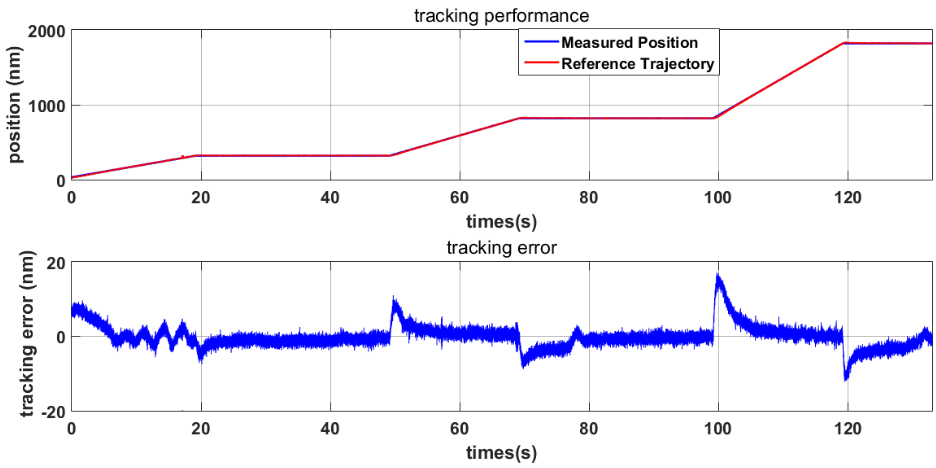

Figure 3-12: Measured position and tracking error for MFC for maximum velocity 50nm/s

Table 3-5: Experimental result for reference ramp tracking with maximum 50nm/s uisng PID, Model-free control, ADRC

Control Method	PID	MFC	ADRC
Maximum of tracking error: ϵ_{max} $[nm]$	54	17	18
Average of the tracking error: ϵ_{avg} $[nm]$	20.1	3.3	3.5
Maximum of tracking error (after $v = 15nm/s$) $[nm]$:	54	17	18
Average of tracking error (after $v = 15nm/s$) $[nm]$:	31.8	3.9	4.0

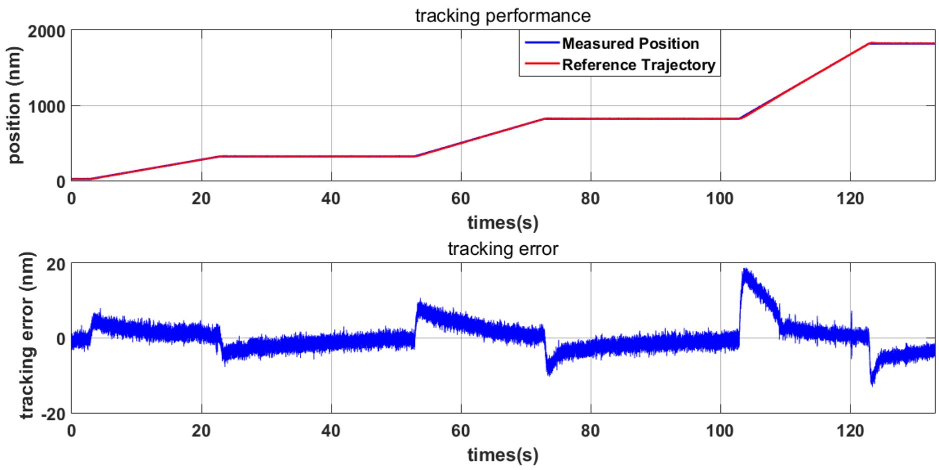

Figure 3-13: Measured position and tracking error for ADRC for maximum velocity 50nm/s

From Figure 3-11, it is obvious that the tracking error of PID increases with the rise of tracking speed. This is due to the limited bandwidth of PID. However, when the tracking velocity is increased to $50nm$, the tracking error of MFC and ADRC do not have a sharp change. MFC has a faster response than PID because MFC has a 'feedforward' mechanism by which the system nonlinearities, as well as disturbances can be compensated. Tuning of MFC is much easier than that of PID, the parameter of MFC can be tuned in a very a broad range without losing stability while PID can easily lose stability due to its narrow parameter set. Due to the existence of compensation mechanism, the error that enters the PID component of MFC method becomes much smaller, which makes tuning of PID parameters of the MFC method quite straightforward. Although decent performance has been obtained by ADRC, tuning of ADRC parameters is a tough and time-consuming task since there are more than 10 parameters to be tuned. In conclusion, the simple MFC method which shows its superiority in handling system nonlinearity and disturbance rejection both from experiment validation and numerical simulation is a good replacement for classical PID for the control of the nano-positioning stage.

3-6 Conclusion

In this chapter, three control methods have been proposed for the control of the nano-positioning stage. For the sake of the comparison, the simulation for robustness analysis has been presented. Three scenarios have been proposed to compare the performance of the controller under sensor noise, model variation and external disturbance. Next, these three control methods have been applied to real setup to test their performance. To sum up, the comparison of three different control methods is as follows:

- **Structure**
  Two main loops can be distinguished in both ADRC and MFC, i.e, compensation loop and output feedback control loop. However, PID only has an output feedback loop. Both of ADRC and MFC can be regarded as a feedback controller plus a feedforward

control. However, the type of connecting feedback controller is not confined, which can be determined by a specific task.

- **Compensation mechanism**
PID does not have a compensation mechanism. For MFC, the system dynamics and disturbances are compensated by a lumped parameter F which is estimated through a local model of the process, while the ADRC method uses an extra state to estimate system dynamics and disturbances and then compensates it. MFC and ADRC have extremely high similarity in structure. The main difference is the method for the realization of dynamics compensation.

- **Parameter tuning**
The good tuning of PID parameter relies on the knowledge of the plant. For mechatronics system, loop shaping in frequency domain is the most common used method. The tuning of MFC parameters is quite straightforward because the existence of compensation mechanism relieves the burden of PID. However, the tuning of ADRC is not an easy job since it has a number of parameters need to be tuned. Due to the nonlinear structure of ESO, tuning of ADRC usually takes some time.

- **Performance of control method**
From the simulation result, it can be seen that both the ADRC and MFC have good robustness. PID shows poor performance of noise suppression, disturbance rejection and resistance to model variation due to its relatively simple structure. The experimental result shows that MFC and ADRC have significant advantage in handling the nonlinear and complex system, which can be promoted to other applications.

Given the above comparison for different control methods from different aspects, the novel model-free control, a simple but effective control method that shows strong robustness and ability to handle nonlinear dynamics, can be a good alternative for general PID method.

Chapter 4

Some explorations for improving current MFC method

In terms of several drawbacks of current model-free control in different applications, some improvements for this method are presented in this chapter. These modifications aim at improving the current method from different aspects. These modifications focus on the practicability without adding too much complexity to the original method. In this chapter, three aspects of modification will be mainly focused: exploration for higher order derivative estimator, improvement of the transient process by tracking differentiator and new ultra-local parameter estimation method. Both numerical simulation and experimental validation for these modifications are presented.

4-1 Some drawbacks for current model-free control method

Though fruitful outcomes in both theory and applications for this method have been obtained in the recent years, several drawbacks which are found in applications still exist and need to be improved. These drawbacks limit the performance of the controller, which arouses our interests to do some explorations on them. Given the relatively low computational load of model-free control, we do not want to add too much complexity to the current method. Applicability and performance will be mainly focused on in this chapter.

M. Fliess et al.[10] mentions the performance of first order model-free control is insufficient for some specific system, especially for the system without the first-order derivative term. J. M. Rodriguez-Fortun et al.[19] mentions the system performance is unsatisfactory due to the lack of inertial terms in the ultra-local model expression and the implementation of higher order ultra-local model is also listed in his future work. However, no existing literature presents the comparison of the performance for second order model-free control and first order model-free control. As for experimental setup, due to the presence of friction which can be expressed as a nonlinear function of velocity ($\alpha\dot{x}$), the first order ultra-local model will not lead to the algebraic loop and instability. The second order model-free control will be applied to the experimental setup to compare with the first order model-free control. As future work, it can be applied to other types of positioning stage which lack friction for the verification and comparison.

In terms of the structure of model-free control, the derivative of the reference signal is obtained by differentiating the reference signal. However, due to the existence of noise, the quality of the derivative of the reference signal gets worse, which can affect the performance of the controller. Besides, it is difficult for the experimental setup to track step reference with large magnitude, thus the combination of tracking differentiator to improve transient process will be necessary. Refer to advantage of other nonlinear control methods, it is of great necessity to introduce a reference signal generator for model-free control, which can provide a high-quality derivative of the reference signal and arrange the desirable transient process. Based on above argument, a nonlinear tracking differentiator will be introduced to improve the quality of the reference signal and transient process for the model-free controller.

The current model-free control utilizes a two-parameters ultra-local model where one of them can be estimated through the estimation of the derivative of the output and the other parameter is a static gain and it is usually fixed arbitrarily. In reality, since the simplified ultra-local model represents the real physical model of which the input gain α and structural parameter F are both time-varying, so the estimation of a single parameter by the algebraic derivation technique is insufficient to obtain the desired performance when the estimation of the second parameter is required. As previously mentioned, model-free control does not perform well enough during the initial transient. J. Villagra et al.[18] attributes it to the choice of input gain α. Therefore, it is necessary to propose a new two-parameters ultra-local model estimation method and compare it with the current method.

In conclusion, aiming at solving the above drawbacks of the current model-free control method, our explorations will be focused on the following three aspects: the higher order ultra-local model, the new reference signal generator and the new parameter estimation method. The performance of new method will be compared with the current method to show its validity in improving the system performance.

4-2 Higher order ultra-local model

Any physical model can be simplified into a two-parameter simple ultra-local model, which works only in a small time range and renews at each sampling time. As (4-1) shows, the core of this model is the estimation of parameter F which relies on the estimation of the derivative of the output that might be corrupted by noise.

$$\hat{F}(k) = \hat{y}^{(n)}(k) - \alpha u(k-1) \tag{4-1}$$

For this case, n is selected to be an integer which is larger than 1. Similar as the derivation of first order derivatives, the higher order derivative estimation also consists in designing FIR filters resolving a classical polynomial approximation of the signal which is usually corrupted by noise. For the sake of conciseness, the complex derivation process is left out. The reader can refer to the part of derivatives of noisy signals in Section 3-1 and [20].

Through (3-14) and (3-15), the estimation of higher order derivative can be derived as follows:

$$y^{(j)}(t) = \sum_{k=1}^{M} \Pi_{j,k} y(t-(k-1)T_s) \tag{4-2}$$

for $j = 0, 1, 2, \cdots, N$. Where

$$\Pi_{j,k} = \frac{(N+j+\nu+1)!(N+1)!}{(MT_s)^j} \sum_{\kappa_1=0}^{N-j} \sum_{\kappa_2=0}^{j} \sum_{i=0}^{\nu+\kappa_1+\kappa_2} \frac{(-1)^{N+i-\kappa_1-\kappa_2}((\frac{k}{M})^{N+i-\kappa_1-\kappa_2+1} - (\frac{k-1}{M})^{N+i-\kappa_1-\kappa_2+1})}{\kappa_1!\kappa_2!i!(N-j-\kappa_1)!(j-\kappa_2)!(N-\kappa_1-\kappa_2)!(\nu-i+\kappa_1+\kappa_2)!(N-\kappa_1+1)(N+i-\kappa_1-\kappa_2+1)} \tag{4-3}$$

With T_s is the sampling time, T is the window width which can be chosen by the practitioner and M denotes the number of summation steps, it holds $M = T/T_s$, N is the order that the signal is approximated by Taylor-series expansion. $\Pi_{j,k}$ is weight fuction of FIR filter.

The rise of order will dramatically increase the computational complexity. For the sake of simplicity, in this thesis, only the second order derivative estimator will be compared with the first order derivative estimator. The parameter for the simulation are selected as follows: $M = 10$, $T_s = 0.001s$, $T = 0.01s$ and $N = 2$. A sinusoidal signal with the magnitude of $30nm$ and frequency of $20rad/s$ is used as the reference signal to test the performance of second order derivative estimators. As the measured output are always corrupted by noise, without losing generality, Gaussian noise with $N(0, 10^{-11})$ is added to the output. Figure 4-1 and Figure 4-2 show the comparison of the estimation from the second order derivative estimator and the result obtained by differentiating the reference signal.

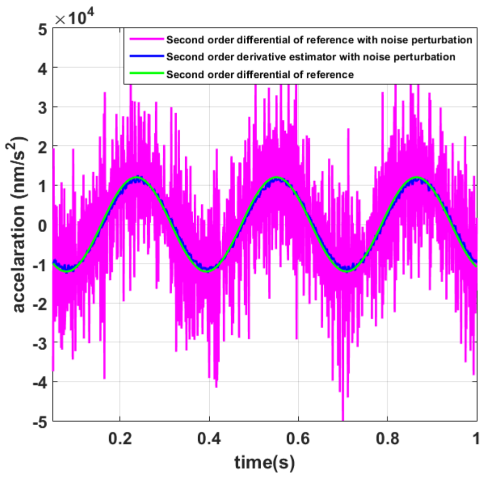

Figure 4-1: The performance of the second order derivative estimator and second order differential of reference with noise perturbation

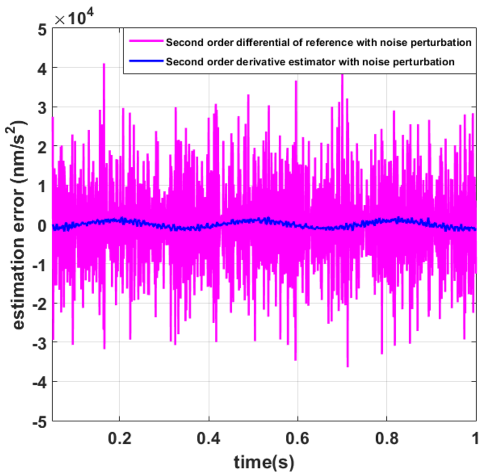

Figure 4-2: The estimation error of the second order derivative estimator and second order differential of reference with noise perturbation

It can be seen that the performance of the second order derivative estimator is much better than that of the differential of the reference signal. Direct differential of the reference signal will amplify the noise, which makes the quality of estimated signal worse. The new derivative estimator can accurately estimate the second order derivative of noisy output, which can be used for our second order model-free control.

4-3 Novel method for structural parameter estimation

The model-free control utilizes a two-parameters ultra-local model where one of them can be estimated through an algebraic method, the other parameter, for simplicity, is a static gain which can be allocated by trial and error. In reality, since the simplified ultra-local model represents the real-life physical model of which the structural parameter α and F are both times varying, so the estimation of a single parameter by the algebraic derivation technique is insufficient to obtain the desired performance when the estimation of the second parameter is required[21]. Thus, it is necessary to develop a new method to estimate the structural parameter of the ultra-local model.

Consider the second order ultra-local model as a regressor [22]:

$$\ddot{y}(t) = H(t)\theta(t) \tag{4-4}$$

where $H(t) = \begin{bmatrix} 1 & u(t) \end{bmatrix}$ and $\theta(t)^T = \begin{bmatrix} F & \alpha(t) \end{bmatrix}$

The estimation of $\hat{\theta}(t)$ can be thought as the solution of the undetermined linear equation. The solution can be written as:

$$\theta(t) = H(t)^{\dagger}\ddot{y}(t) + (I_2 - H(t)^{\dagger}H(t))\xi(t) \tag{4-5}$$

where:

- $H(t)^{\dagger}$ denotes the pseudo-inverse of $H(t)$, namely it fulfills the relationship $H(t)H(t)^{\dagger}H(t) = H(t)$
- $\xi(t)$ is an arbitrary 2-dimensional vector.

This solution form can be utilized to calculate the $\hat{\theta}(t)$, since $H(t)$ is full row rank, that is $H(t)H(t)^T$ is not singular, so $H(t)^{\dagger}$ is a right inverse of H(t). We have the following expression: $H(t)^{\dagger} = H(t)^T(H(t)H(t)^T)^{-1}$. Thus, the $H(t)^{\dagger}$ can be ontained:

$$H(t)^{\dagger} = \frac{1}{1+u(t)^2}\begin{bmatrix} 1 \\ u(t) \end{bmatrix} \tag{4-6}$$

$H(t)^{\dagger}$ is Subsitituted into (4-5), $\xi(t)$ is selected as $\begin{bmatrix} 1 \\ 2 \end{bmatrix}$, the estimator can be read as:

$$\begin{aligned} \hat{\theta}(t) =& \frac{1}{1+u(t)^2}\left(\ddot{y}(t)\begin{bmatrix} 1 \\ u(t) \end{bmatrix} + \begin{bmatrix} u(t)^2 - 2u(t) \\ 2 - u(t) \end{bmatrix}\right) \\ =& \frac{1}{1+u(t)^2}\begin{bmatrix} \ddot{y}(t) + u(t)^2 - 2u(t) \\ \ddot{y}(t)u(t) + 2 - u(t) \end{bmatrix} \end{aligned} \tag{4-7}$$

Which leads to:

$$
\begin{aligned}
\hat{F}(t) =& \frac{\ddot{y}(t) + u(t)^2 - 2u(t)}{1 + u(t)^2} \\
\hat{\alpha}(t) =& \frac{\ddot{y}u(t) + 2 - u(t)}{1 + u(t)^2}
\end{aligned}
\tag{4-8}
$$

It is clear that the estimated $\hat{F}(t)$ and $\hat{\alpha}(t)$ satisfy the ultra-local model (4-4), however $\xi(t)$ is arbitrary 2-dimensional vector, the estimation set of $\theta(t)$ is infinite.

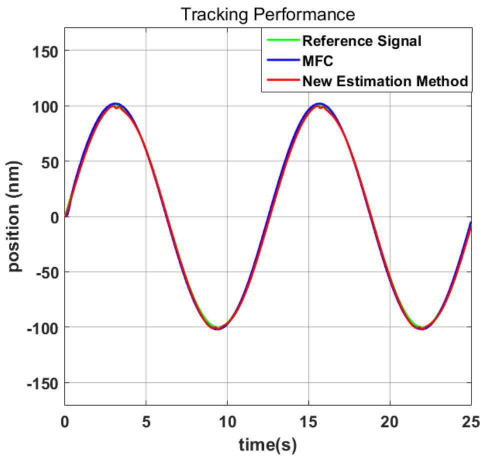

Figure 4-3: The comparison of tracking performance for MFC and MFC with new estimation method

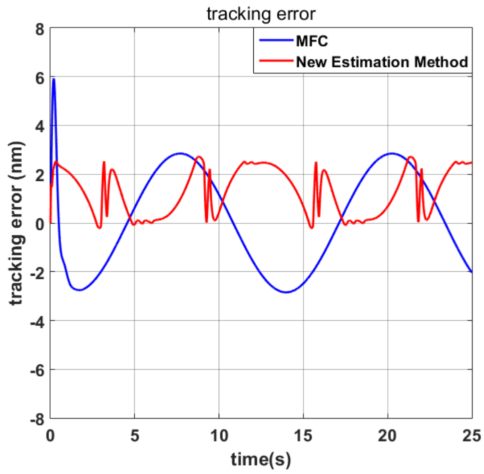

Figure 4-4: Tracking error of MFC and MFC with new estimation method

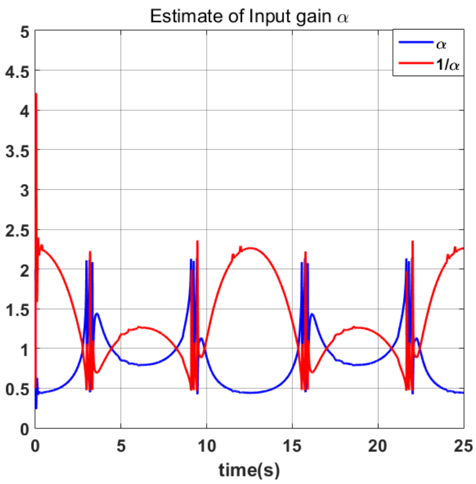

Figure 4-5: The estimation of α

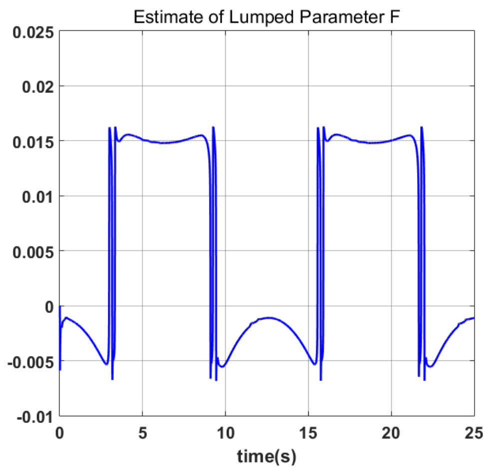

Figure 4-6: The estimation of F

A sinusoidal signal with the magnitude of $100nm$ is used to test the new estimation method. As can be seen in Figure 4-3 and Figure 4-4, the tracking performance of model-free control with the new estimation method is better than model-free control, which confirms the effectiveness of the new estimation method. This method provides the possibility of estimation of two structural parameters at the same time. However, from Figure 4-5, the input gain α varies between 0.5 to 2.5. As shown in Figure 4-7, the $\frac{1}{\alpha}$ is the scaling factor of the system, thus frequent change of α will deteriorate the robustness of the system. The variation of α gets larger when this method is applied to the real setup, which is due to the effect of external disturbances and noise. Given the robustness of the system, the drastic change of α is not what we expected. Thus, in the future work, the variation of α should be bounded in a reasonable range so that the robustness of the system can be guaranteed.

4-4 Improvement of transient process by tracking differentiator

The nonlinear tracking differentiator which is a component of ADRC has been introduced in Section 3-2. Given the advantage and properties of the nonlinear tracking differentiator, the tracking differentiator can be introduced to our model-free control to improve the transient process. As previously mentioned, the model-free control uses the derivative of the reference signal, which will amplify the contaminated noise and decrease the quality of the signal. Tracking differentiator provides two reference signals $r_1(t)$ and $r_2(t)$, such that $r_1(t) = r(t)$ and $r_2(t) = \dot{r}(t)$. The parameter δ can be determined empirically to improve the transient process. δ is named as "velocity factor" and h is the sampling period. There is a tradeoff between the tracking and robustness. Large δ is helpful to fast the transition and tracking while probably decreasing the robustness at the same time[23]. The formula of nonlinear tracking differentiator is summarized as follows:

$$\begin{cases} r_1(k+1) = r_1(k) + hr_2(k) \\ r_2(k+1) = r_2(k) + hfhan(r_1(k) - r(k), r_2(k), \delta, h) \end{cases} \tag{4-9}$$

Where the function $hfhan(r_1(k) - r(k), r_2(k), \delta, h)$ can be expressed as follows:

$$fhan(x_1, x_2, \delta, h) = -\begin{cases} \delta sign(a), & |a| > d \\ \delta \dfrac{a}{d}, & |a| \le d \end{cases} \tag{4-10}$$

where a and d will be determined by

$$a = -\begin{cases} x_2 + \dfrac{(a_0 - d)}{2} sign(y) & |y| > d_0 \\ x_2 + \dfrac{y}{h} & |y| \le d_0 \end{cases} \tag{4-11}$$

with

$$\begin{cases} d = \delta h \\ d_0 = hd \\ y = x_1 + hx_2 \\ a_0 = \sqrt{d^2 + 8\delta |y|} \end{cases} \tag{4-12}$$

As step signal is used as the reference to test the improvement of the transient process by the tracking differentiator. From Figure 4-8, it can be seen that with the increase of δ, the transition is faster. Figure 4-9 gives more clear demonstration. With the rising of δ, the

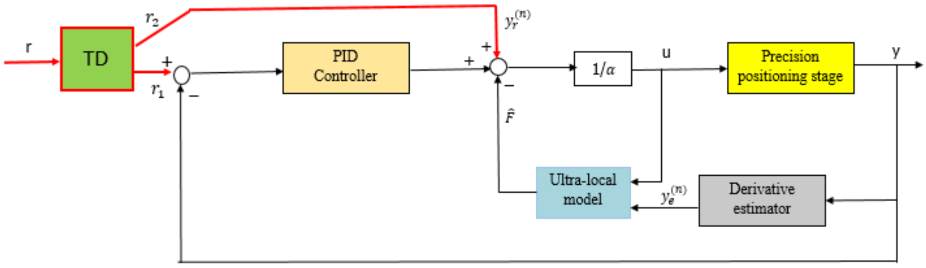

Figure 4-7: Block diagram of TD plus MFC

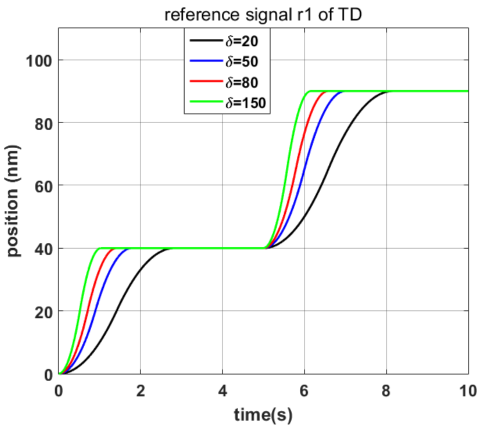

Figure 4-8: Reference r_1 of TD

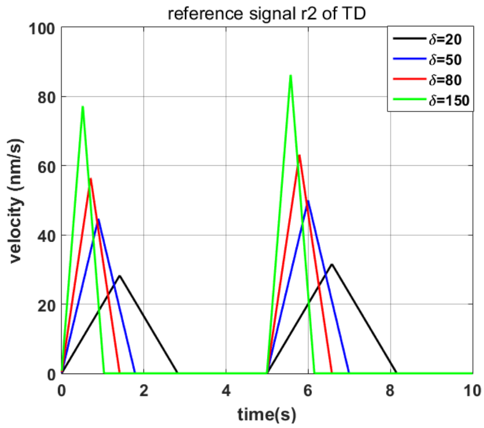

Figure 4-9: Reference r_2 of TD

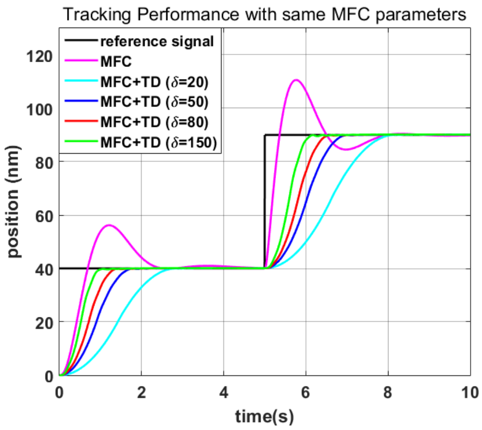

Figure 4-10: Tracking performance for MFC and MFC plus TD with same controller parameters

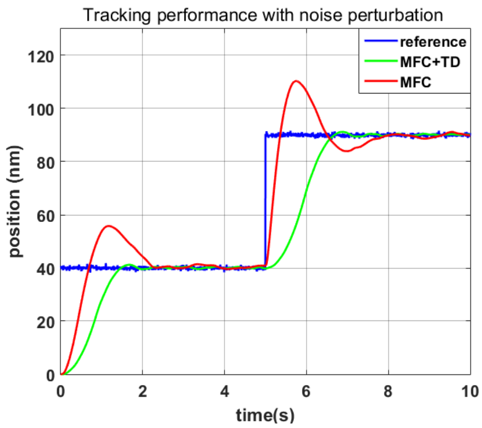

Figure 4-11: Tracking performance for MFC and MFC plus TD with noise perturbation

transition will have a larger rising and descending acceleration and the transition period will become shorter. Figure 4-10 shows the comparison of tracking performance for model-free control alone and model-free control with nonlinear tracking differentiator. It should be noted that the same model-free control parameters are used for all the scenarios. The introduction of the nonlinear tracking differentiator can dramatically improve the transition process. A larger overshoot can be avoided by adding the tracking differentiator to the model-free control. When Gaussian noise $N(0, 10^{-11})$ is added to the reference, as can be seen in Figure 4-11, the model-free control with tracking differentiator has less tracking error compared with model-free control alone. Tracking differentiator can filter the noise thus the system will be less affected by the reference noise. In terms of the above advantages, we introduce the tracking differentiator to our model-free control and experiment validations are shown in the subsequent section.

4-5 Experiment validations and result

4-5-1 The comparison of performance for second-order MFC and first-order MFC

The second order model-free control has been proposed in this chapter, the experiment result for this method is presented here. For the sake of comparison, the same ramp reference signal as mentioned in Section 3-5 is used to test the performance of second-order model-free control and make a comparison with the first order model-free control. The maximum tracking velocity for Figure 4-12 and Figure 4-13 are $15nm/s$ and $50nm/s$, respectively. The performance of first order model-free control was presented in Figure 3-9 and Figure 3-12, Table 4-1 and Table 4-2 summarize the tracking performance of second order model-free control and first order model-free control.

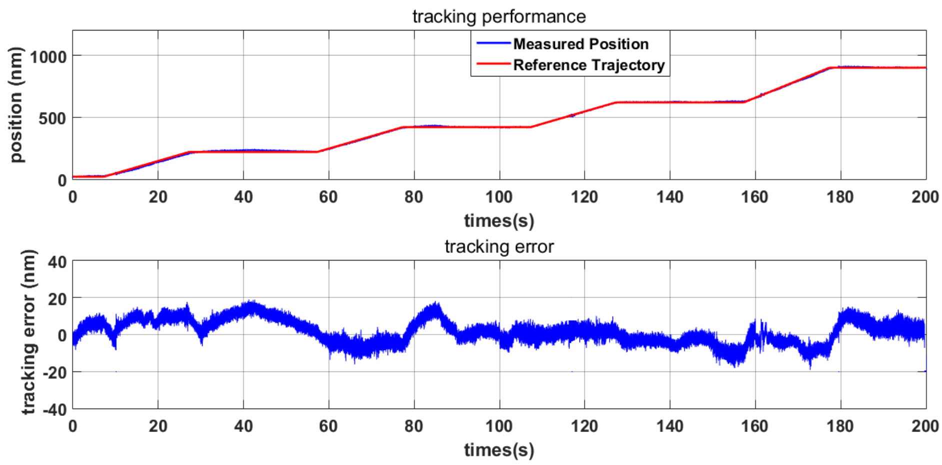

Figure 4-12: Measured position and tracking error for second-order MFC for maximum velocity 15nm/s

The above result shows that the performance of first order model-free control is slightly better than that of second order model-free control because the positioning system needs more time to react for the variation of acceleration of output. The system has larger inertia for second order model-free control so that the system performance may be poorer in the initial stage. However, the advantage of second order model-free control is that it can achieve faster tracking velocity than the first order model-free control.

As can be seen in Table 4-2, second order model-free control has less maximum of tracking error while the average of tracking error is considerably larger than first order model-free

Table 4-1: Experimental result for reference ramp tracking with maximum 15nm/s uisng 1^{st} order MFC and 2^{nd} order MFC

Parameter	2^{nd} order MFC	1^{st} order MFC
Maximum of tracking error: ϵ_{max} $[nm]$	18	14
Average of the tracking error: ϵ_{avg} $[nm]$	4.5	3.9
Maximum of tracking error (after $v = 15nm/s$) $[nm]$:	12	10
Average of tracking error (after $v = 15nm/s$) $[nm]$:	4.4	3.9

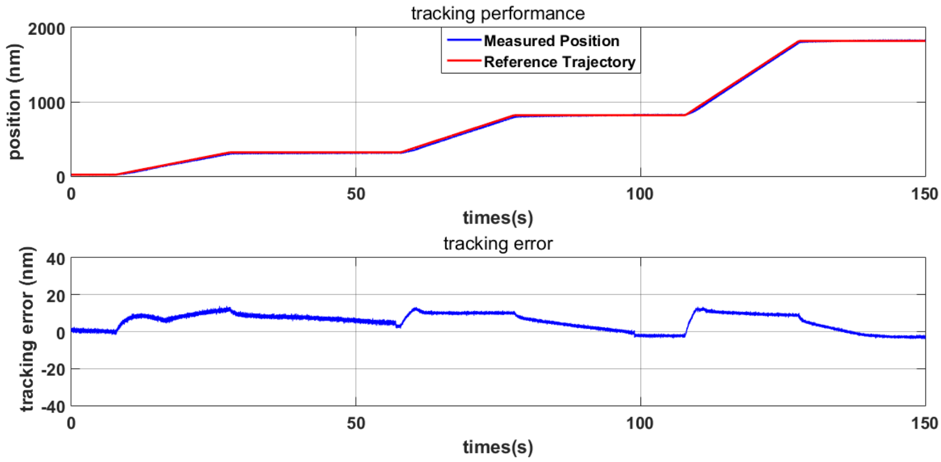

Figure 4-13: Measured position and tracking error for second-order MFC for maximum velocity 50nm/s

Table 4-2: Experimental result for reference ramp tracking with maximum 50nm/s uisng 1^{st} order MFC and 2^{nd} order MFC

Parameter	2^{nd} order MFC	1^{st} order MFC
Maximum of tracking error: ϵ_{max} $[nm]$	14	17
Average of the tracking error: ϵ_{avg} $[nm]$	5.9	3.3
Maximum of tracking error (after $v = 50nm/s$) $[nm]$:	14	17
Average of tracking error (after $v = 50nm/s$) $[nm]$:	6.6	3.9

control. It is difficult to compare the second-order model-free control with the first order model-free control from the mathematical way as any higher order system which is expressed by a group of differential equations can be simplified and represented by the first or second order local model. The advantage of each local model may vary in terms of the different applications. As previously discussed, a frictionless air bearing stage performs poorly using the first order model-free control because an algebraic loop may emerge as the model lacks the first order term. Thus, the first order model-free control and second-order model-free control can be a supplement for each other. We can test both of them in a specific setup and decide which method we will use.

4-5-2 The performance of the combination of MFC and TD

To test the improvement of the transient process of model-free control by introducing a tracking differentiator, a step signal with the magnitude of $200nm$ is used. It should be mentioned that step signal is difficult to track for this setup, which is probably due to the manufacturing process. The system frequently loses stability at the initial stage when a step reference signal with larger magnitude is added. On the contrary, line tracking can be easily achieved. The tracking differentiator will generate the new reference r_1 and its derivative r_2 for a controller in terms of different dynamic characteristic requirements, which will greatly improve the system performance in the transient state.

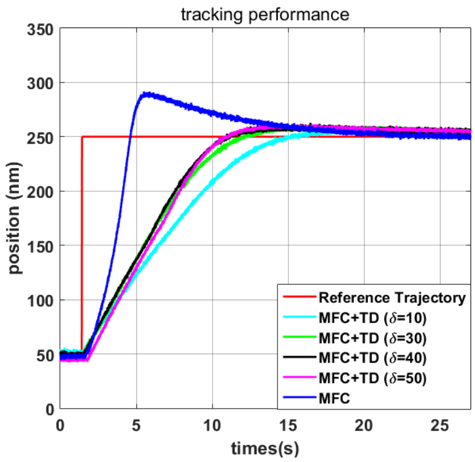

Figure 4-14: Measured tracking performance for MFC and MFC plus TD with same controller parameters

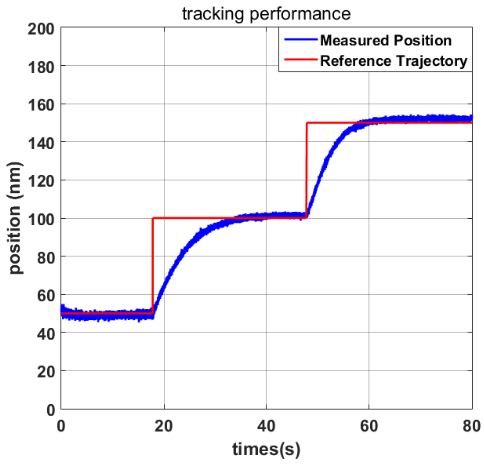

Figure 4-15: Measured performance for MFC plus TD

Table 4-3: Experimental result for step tracking for MFC and MFC plus TD with different velocity factors

Parameter	without TD	TD (δ=10)	TD (δ=30)	TD (δ=40)	TD (δ=50)
Rise time: t_r $[s]$	2.8	10.6	8.2	6.5	6.4
Settling time: t_s $[s]$	13.5	12.1	10.2	8.8	8.6
Maximum Overshoot M_r	17.5%	1%	2%	2%	3%
Peak time t_p $[s]$	3.9	14.2	12.8	10.3	10.2

As can be seen in Figure 4-14, the combination of tracking differentiator and model-free control can dramatically improve the performance in the transient state. Model-free control has a large overshoot which can be avoided by introducing the nonlinear tracking differentiator. The simulation result in Section 4-4 has shown that the overshoot cannot be totally avoided if the disturbances and noise exist, however, the excessive overshoot can be avoided by the tracking differentiator and simultaneously keep a reasonable rise speed. From the experimental result, when the parameter δ increases from 30 to 50, the change in transient process is not obvious, which is different from the simulation result. This is due to the existence of noise and disturbances in the real scenario. $\delta = 10$ has relatively longer rise time but the overshoot is the least. With this velocity factor, the performance for tracking the multi-step reference with the magnitude of $50nm$ is shown in Figure 4-15. The system has less than 1% overshoot throughout the tracking process, which illustrates the effectiveness of adding the tracking differentiator.

4-6 Conclusion

This chapter proposes some modifications for current model-free control in terms of the drawback of the current method. Initially, the first order model-free control may fall into the algebraic loop if the model lacks the first order term. The design method for second order model-free control is presented in this chapter. For the sake of comparison, second order model-free control is simulated and tested in the real experiment. The second order model-free control and the first order model-free control can be a supplement for each other, the superiority of each method will depend on the dynamic of a specific system. Then, as the input gain α is estimated by trial and error for the current method, we propose a new estimation method which can estimate the structrual parameters α and F at the same time. The simulation result is presented. Although the simulation result shows that the performance of the new method is better than the current method, the new method still needs to be enhanced in the robustness aspect. Finally, since the step signal is difficult to track for this setup, a nonlinear tracking differentiator is added to improve the transient process. Both the simulation and experiment results verify the effectiveness of this new method.

Chapter 5

The learning enhanced model-free control

5-1 Introduction

Though the application of novel model-free control dramatically improves the tracking accuracy of positioning stage. The tracking performance can be further improved by the combination of other techniques, such as feedforward model and iterative learning control. The numerical and experimental results are presented to show the effectiveness and validness of the method.

For precision mechanical motion systems, friction can sharply deteriorate the tracking performance of the system. Possible unwanted consequences caused by friction are steady-state errors, limit cycling and hunting. In motion control, a possible way to minimize the influences of friction is to compensate for it. As previously mentioned, our model-free control has a 'feedforward' mechanism, the nonlinearity as well as system dynamics is compensated through an estimated linear model which renews at each sampling time. However, this friction compensation method does not rely on the friction model, it is not as precise as model-based friction compensation. In this chapter a feedforward model which can predict the required force for pre-sliding motion is added to cancel the nonlinear pre-sliding friction and reduce the control effort.

As nano-positioning stage usually operates the repetitive tasks like scanning or detection, iterative learning control is combined with model-free control to remove the repetitive error and disturbances. Through 'learning' the tracking error cycle by cycle, the tracking accuracy of new method can be dramatically improved in comparison with model-free method alone. The combination of model-free control and iterative learning control will be discussed in this chapter.

5-2 Presliding friction feedforward

As preciously illustrated, friction is generally divided into two regimes: pre-sliding and full-sliding. For our experimental nano-positioning stage, due to its relatively low speed and high resolution, the motion of mover is generally in the pre-sliding regime where the pre-sliding friction is the dominant factor which can affect the system performance. Section 2-2 illustrated that the input force generated by the actuator is below the stiction limit, thus the motion of stage belongs to the presliding regime.

Pre-sliding is considered as the elastic and plastic deformation of a contact due to an applied shear force below the stiction limit. The factor of pre-sliding regime is usually neglected for general motion control but is essential for the control in nano-scale tracking accuracy. A feedforward model proposed by [1] is applied to our experimental setup, which can compensate for the required force to realize desired tracking motion in pre-sliding regime. This simple model does not need complex numerical identification and the effectiveness of the method is verified by the experiment.

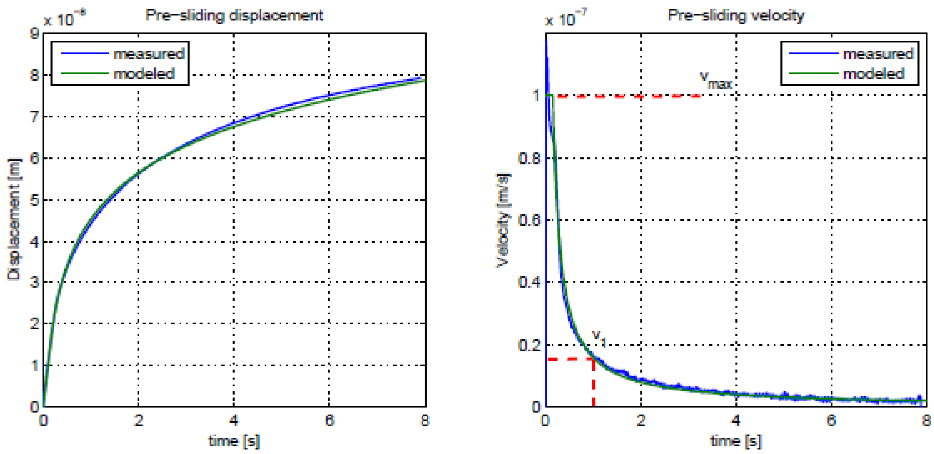

Figure 5-1: Measurement and experimental model of the plastic part of the pre-sliding displacement and velocity[1]

P. Dupont et al.[24] shows the pre-sliding displacement consists of an elastic and plastic part. As the total stiffness of the system is constant, the elastic displacement x_e is a function of applied force F. The plastic displacement is calculated by integrating the pre-sliding velocity v_p over time, so the total displacement equals to:

$$x_t = x_e + x_p = \frac{F}{k} + \int v_p dt \tag{5-1}$$

So the necessary force to achieve a certain displacement in the pre-sliding regime is calculated by (5-2):

$$F = kx_e = k(x_t - x_p) = k(x_t - \int v_p dt) \tag{5-2}$$

Now the problem lies in the calculation of pre-sliding velocity v_p. As the right of Figure 5-1 shows, the plastic part of the pre-sliding velocity v_p has a hyperbolic shape according to:

$$v_p = \frac{v_1}{t}\Big|_{v_{max}} \tag{5-3}$$

where v_1 is the velocity after 1 second and v_{max} is the maximum pre-sliding velocity. The plastic pre-sliding displacement x_p is found via integration:

$$x_p = \int v_p dt = \int \frac{v_1}{t} dt = v_1 \ln(t) + C \tag{5-4}$$

(5-3) will be rewritten into a form where the pre-sliding velocity is a function of displacement, rather than time. t can be calculated from (5-4)

$$t = \exp \frac{x_p - C}{v_1} \tag{5-5}$$

substituting (5-5) in (5-3) obtains

$$v_p = \frac{v_1}{\exp \frac{x_p - C}{v_1}} \Big|_{v_{max}} \tag{5-6}$$

Where the integration constant C can be found from the intersection of the two velocity regimes. It is shown as the knee-point between the v_{max} line and the hyperbolic velocity curve in Figure 5-1. At this point the velocities are equal:

$$v_{max} = \frac{v_1}{t} \tag{5-7}$$

and displacement satifies:

$$v_{max} t = v_1 \ln(t) + C \tag{5-8}$$

From (5-7) the time at which the two functions intersect can be found:

$$t = \frac{v_1}{v_{max}} \tag{5-9}$$

which can be substituted in 5-8, C can be obtained by (5-10):

$$C = v_{max} t - v_1 \ln(t) = v_1 - v_1 \ln\left(\frac{v_1}{v_{max}}\right) \tag{5-10}$$

By identifying v_1 and v_{max} as a function of applied force, and place them in a lookup table, the model can be used to predict the plastic pre-sliding displacements under varying force condition. The model has been verified through experiment and it is valid for all force amplitudes below the stiction limit.

5-3 Learning enhancement compensation

Iterative learning control is an approach to improve the tracking performance of the system which operates the repetitive tasks. The basic ILC is a feedforward control approach which utilizes the past error information to improve the tracking performance. It is a memory-based scheme which needs to store the tracking errors and control efforts of previous repetitions in order to construct the control efforts of the present cycle. In this section, iterative learning control is combined with the previously mentioned model-free control to further improve the tracking performance of positioning stage.

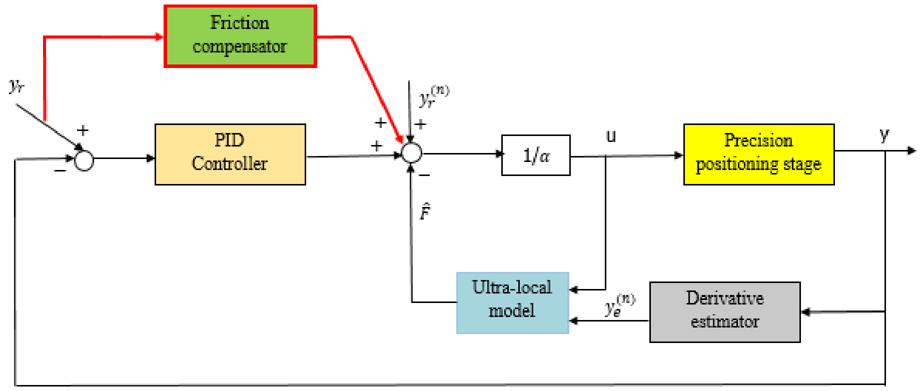

Figure 5-2: Block diagram of MFC plus feedforward

5-3-1 The combination of model-free control and iterative learning control

The general control law of general ILC is shown in (5-11).

$$u_{j+1}(k) = Q(z)[u_j(k) + L(z)e_j(k)] \tag{5-11}$$

where the subscript j reflects the iteration number of the process. The time index ranges from 0 to $N-1$. $Q(z)$ is usually defined as a low pass filter to add robustness and $L(z)$ is defined as learning function [25]. The structure of iterative learning control is shown in Figure 5-3.

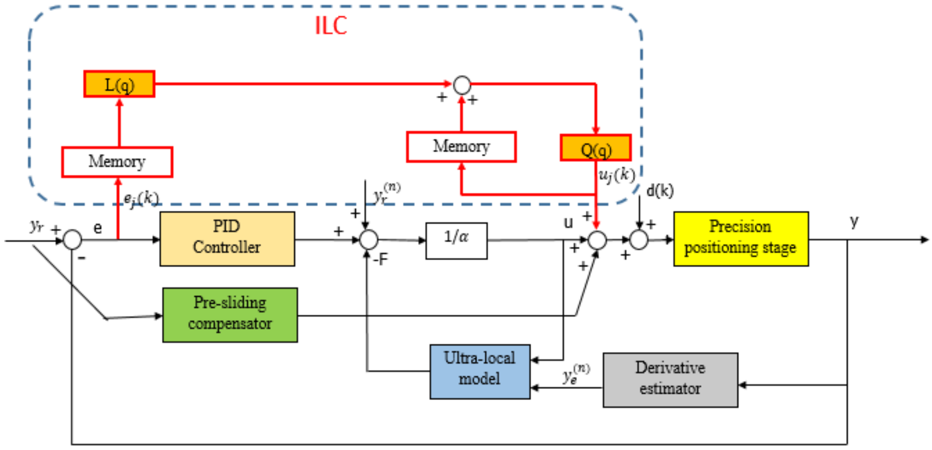

Figure 5-3: Structure of control method

Given the relatively simple structure of model-free control, P-type Iterative learning control is selected to combine with model-free control. P-type iterative learning control is proven to be a robust and efficient control method in many practical applications. A forgetting factor α is introduced to increase the robustness of P-type algorithm against noise, initialization error and fluctuation of system dynamics [26]. The discrete-time control law of P-type ILC [27].

$$u_{j+1}(k) = (1-\beta)u_j(k) + k_p e_j(k+m) \tag{5-12}$$

where m is the number of step advances which typically equals the delay of the system. k_p is the proportional gain. The Q-filter for P-type ILC is set to 1. β is the forgetting factor. P-type Iterative learning control does not need much plant knowledge and it is easy to implement and tune, which corresponds to the characteristics of model-free control [28].

The block diagram of the new combinative method is shown in Figure 5-3. Model-free control will decrease the non-repetitive error and stabilize the system while iterative learning control can be a supplement for model-free control to compensate the repetitive error and improve the tracking performance. Iterative learning control stores and utilizes the tracking error of the last cycle to construct the control effort of the present cycle, thus the tracking error can be reduced from cycle to cycle. This new method is verified by numerical simulation and experiment.

5-3-2 Simulation for new control method

To test enhancement of MFC by introducing ILC, a triangular signal is used as repetitive tracking reference which is shown in Figure 5-4, In the simulation, disturbances include the repetitive disturbance with the magnitude of 0.1A and Gaussian white noise with $N(0, 10^{-11})$ which is non-repetitive. Figure 5-5 shows a comparison of the performance for MFC alone and the proposed new control method.

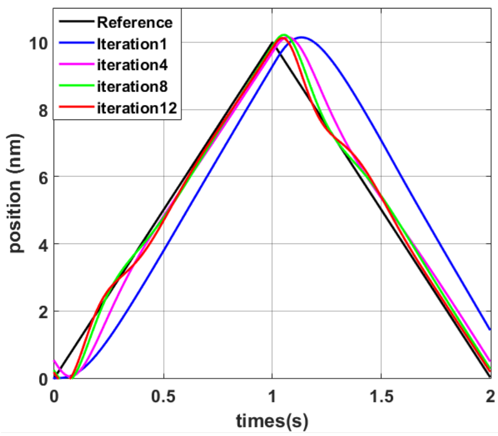

Figure 5-4: Tracking performance for MFC plus ILC for different Iterations

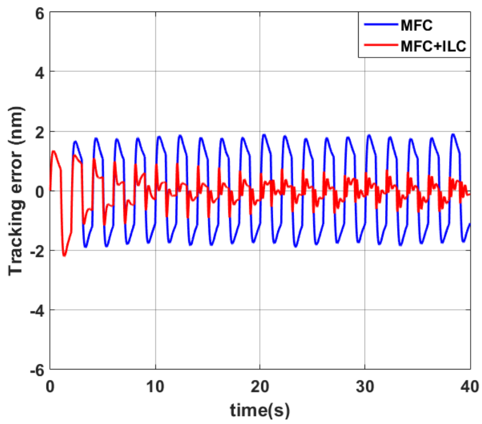

Figure 5-5: Comparison of tracking error for MFC and MFC plus ILC with the disturbance perturbation

It can be seen that the proposed control scheme has a better performance than model-free control alone because iterative learning control can effectively eliminate the repetitive disturbances. The tracking error declines with the increase of iterations. Model-free control can eliminate the non-repetitive tracking error while iterative learning control will learn from repetitive disturbance by iterations and eliminate the repetitive disturbance. Figure 5-6 shows the two norm of tracking error. As can be seen in the graph, the tracking error in iteration 20 is 0.18 while it is 1.12 in the first iteration.The tracking error decreases significantly with the existence of iterative learning control. The simulation result shows with the combination of this simple method, the tracking accuracy of model-free control can be significantly improved.

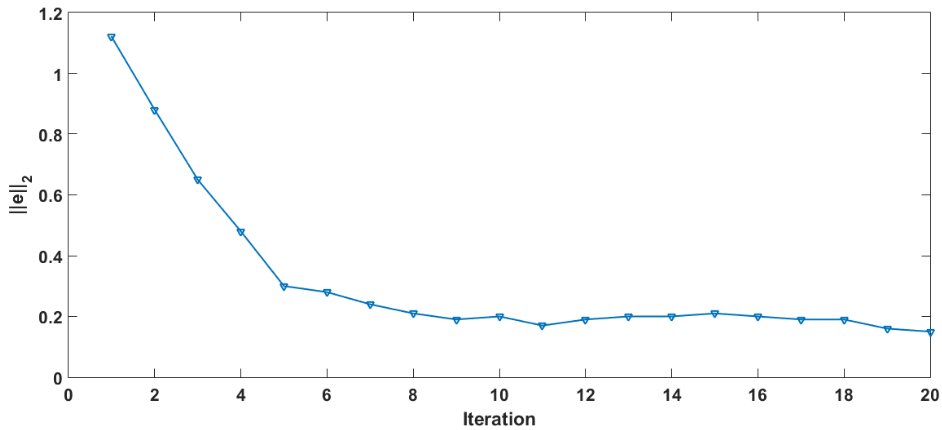

Figure 5-6: Two-norm of tracking errors versus iteration for MFC plus ILC

5-4 Experimental validations and result

In Figure 3-8, 3-9 and 3-10 in Section 3-5, the experimental results for PID, MFC and ADRC for maximum $15nm/s$ have been presented. The same reference signal in Section 3-5 is used to test the performance of model-free control plus a feedforward model. The measured position and position tracking errors are recorded. To avoid repetition, only tracking performance for model-free control plus feedforward is given. Table 5-1 lists a summary of the tracking experiment results for model-free control plus feedforward and the previously mentioned three control methods.

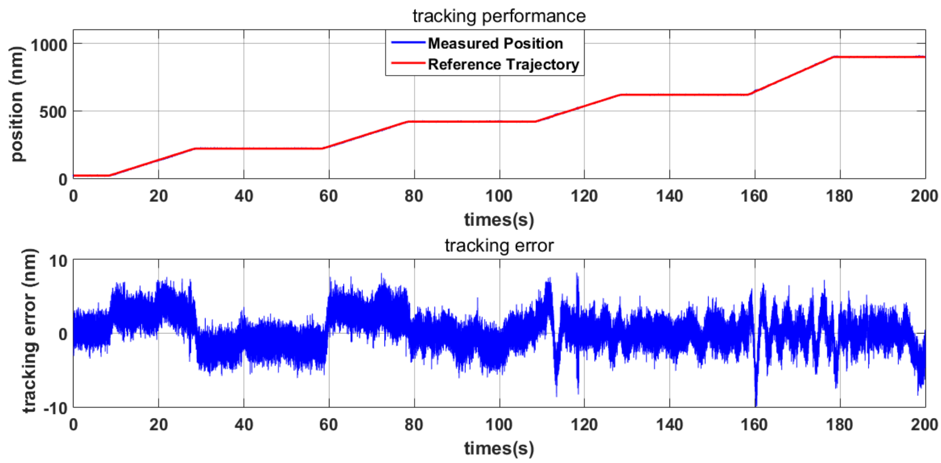

Figure 5-7: Measured position and tracking error for MFC plus feedforward for maximum velocity 15nm/s

The result shows the model-free control with feedforward has less tracking error in comparison with the other three control methods. Compared with model-free control, the maximum tracking error reduces by 50% for model-free control plus feedforward. The tracking error for model-free control plus feedforward does not even increase when the tracking velocity is increased to $15nm/s$. Thus, we can conclude that the introduction of feedforward improves

Table 5-1: Experimental result for reference ramp tracking with maximum 15nm/s uisng PID, Model-free control, ADRC and Model-free control plus feedforward

Control method	PID	MFC	ADRC	MFC+FF
Maximum of tracking error: ϵ_{max} $[nm]$	48	14	9	7
Average of the tracking error: ϵ_{avg} $[nm]$	12.4	3.9	3.3	2.1
Maximum of tracking error (after $v = 15nm/s$) $[nm]$:	48	10	9	4
Average of tracking error (after $v = 15nm/s$) $[nm]$:	17.7	3.9	3.5	2.0

the tracking accuracy of model-free control. The tracking error can be reduced to around $2nm$, which is a superb result for the application of positioning stage.

As we mentioned in Section 3-5, the new reference signal with higher tracking velocity is used to test the performance of model-free control plus feedforward control. The maximum of tracking velocity for this new reference signal is $50nm/s$, the result is shown in Figure 5-8 and Table 5-2.

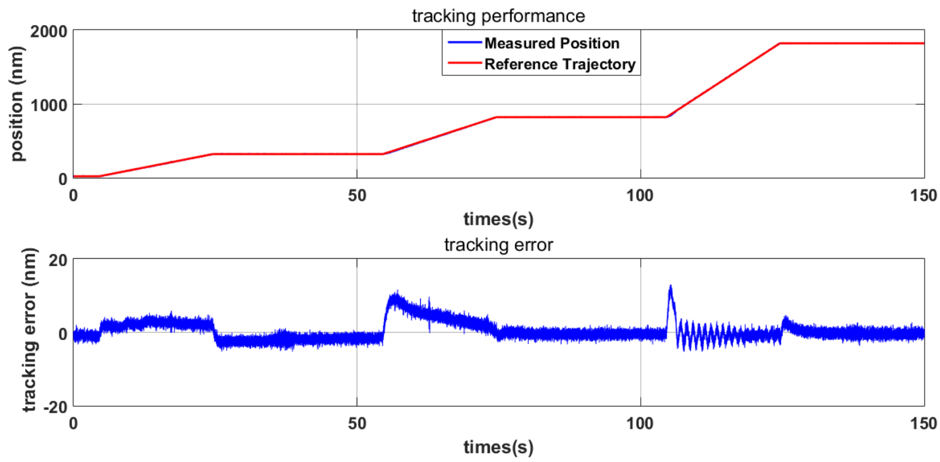

Figure 5-8: Measured position and tracking error for MFC plus feedforward for maximum velocity 50nm/s

Table 5-2: Experimental result for reference ramp tracking with maximum 50nm/s uisng PID, Model-free control, ADRC and Model-free control plus feedforward

Control Method	PID	MFC	ADRC	MFC+FF
Maximum of tracking error: ϵ_{max} $[nm]$	54	17	18	12
Average of the tracking error: ϵ_{avg} $[nm]$	20.1	3.3	3.5	2.2
Maximum of tracking error (after $v = 15nm/s$) $[nm]$:	54	17	18	12
Average of tracking error (after $v = 15nm/s$) $[nm]$:	31.8	3.9	4.0	2.1

As can be seen in Table 5-2, the tracking error for model-free control plus feedforward remains almost constant when the tracking velocity is increased to $50nm/s$. Model-free control has a compensation mechanism and friction has been incorporated, however, since the ultra-local model is a linear simplified model of the real plant which is not precise, the introduction of feedforward which contains the precise model for friction is extremely necessary. The experimental results also confirm this. The tracking error almost reduces with 40% in comparison with model-free control alone. The limitation of this method is that it relays on the experimental result, thus this model cannot be directly taken from one specific setup to another. Besides, this model only approximates the pre-sliding friction and full sliding friction is not involved. However, for our experimental setup, due to its relatively low speed, the motion is mainly in the pre-sliding regime.

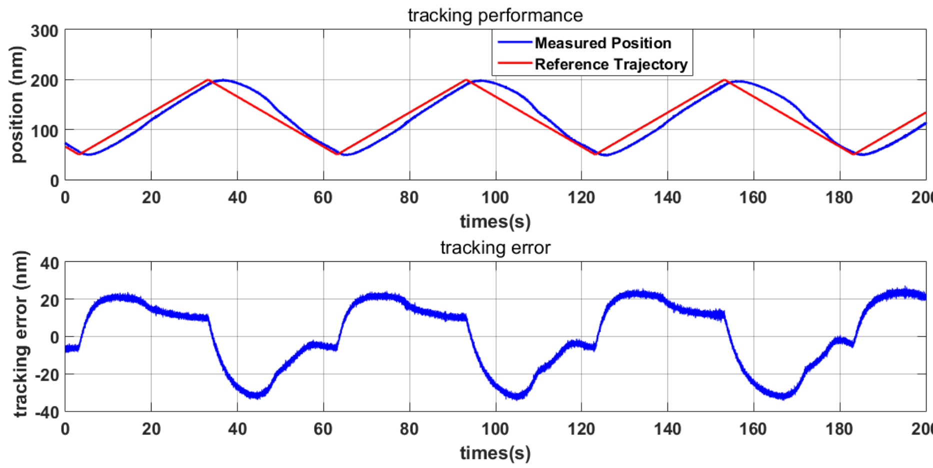

Figure 5-9: Model-free control for triangular wave tracking

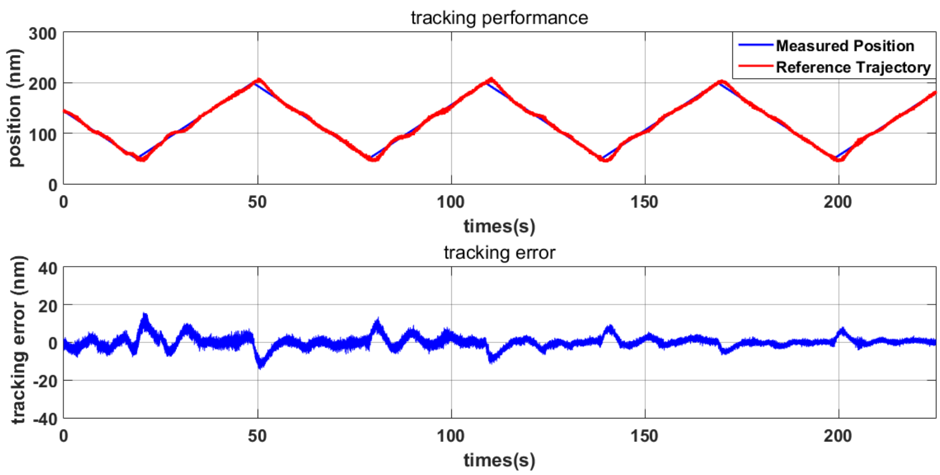

Figure 5-10: Model-free control with Iterative learning control plus feedforward for triangular wave tracking

To evaluate the performance of learning enhanced model-free control, a triangular wave reference signal is used to make a comparison with model-free control. The cycle of the triangular wave signal is $60s$. Figure 5-9 and 5-10 respectively illustrate the tracking performance of model-free control and the combination of model-free control, iterative learning control and feedforward control.

As can be seen in Figure 5-9, the maximum tracking error is constant in each cycle, which demonstrates that model-free control does not have the capability to eliminate the repetitive error. It is a common drawback for general feedback control. Figure 5-10 clearly shows the advantage of iterative learning control, the tracking error decreases by cycle and cycle. The maximum tracking error in the fourth cycle is 25% of that in the first cycle. In summary, the combination of model-free control, feedforward control and iterative learning control can considerably improve the tracking performance and tracking accuracy, therefore it is a good option for the control of the positioning stage.

5-5 Conclusion

In this chapter, two other control methods are introduced to make a combination with model-free control. Feedforward control can precisely compensate the pre-sliding friction and reduce the control effort. The experimental result shows that the addition of feedforward can reduce around 40% of the tracking error for model-free control. The iterative learning control can eliminate the repetitive error and disturbances for model-free control. The advantage of the combination of iterative learning control, feedforward control and model-free control is quite obvious from the simulation and experimental result. This simple and effective control method can also be applied to other systems and applications. It should be noted that the enhancement of performance is more remarkable if this new method is applied to applications where repetitive disturbance is a dominant factor. For example, the motor drived positioning stage.

Chapter 6

Conclusion and Future work

6-1 Conclusion

In the last decades, high precision positioning systems have been widely used in a variety of applications. How to improve the tracking performance and the tracking accuracy of positioning stage became popular in scientific research. The performance of traditional PID which still dominates the precision motion system industry is far from satisfactory. Our work is based on above fact. In this thesis, the application of newly proposed model-free control to the nano-positioning stage is focused. The simulation and experiment results in the thesis have shown its superiority in the control of nonlinear systems. Based on this method, some simple but effective techniques are added to improve the current method and compensate for the friction and disturbances. The experimental validations illustrate that with this simple control structure, the excellent tracking accuracy and insensitivity to disturbance are ensured.

Control of positioning stage

The experimental setup shows the highly nonlinear dynamics due to the existence of friction. Besides, the accurate modeling and identification for the positioning stage are difficult and the high sampling rate set a higher requirement for the real-time capability of the control method. Based on above requirement, a novel model-free control which provides an efficient solution to the nonlinear system is selected and developed. For the sake of comparison, the classical PID and ADRC which have similarities of MFC are proposed, simulated and applied to the experimental setup. In order to test the robustness issues for three different control methods, three scenarios are proposed and simulated, namely: sensor noise, model variation and external disturbance. The simulation shows that the MFC and ADRC have strong ability in disturbance rejection which is due to the existence of compensation mechanism by which the disturbance is estimated and eliminated. Model-free control has the decent capability of sensor noise rejection, however, it is weaker than ADRC. Then, three control methods are applied to the real setup. The experimental results illustrate that the model-free control is able to reduce more than 50% of the tracking error compared to PID. The satisfactory tracking performance is obtained by model-free control, the average tracking error is below $5nm$.

The model-free control provides us with an effective option for the control of the nonlinear system. It is a good replacement of general PID method in the future.

Improvement of MFC by simple modifications or adding new techniques

Some drawbacks of current model-free control methods have been found through the simulations and experiments. Targeting at resolving these drawbacks, several modifications for the current method have been explored and implemented. The second order derivative estimator was developed in this thesis, thus we can compare the performance of second order model-free control with that of the first order. The experimental result verifies that the performance of the first order model-free control is slightly better than the second order model-free control. However, the result does not have generality as it largely depends on the dynamic of a specific system. The first order model-free control and the second order model-free control can be a supplement for each other. Since the setup frequently fails in the step signal tracking, a nonlinear tracking differentiator is proposed to combine with model-free control to improve the transition process. With the combination of TD, the setup can easily track the step signal with less overshoot and transient process can be tuned by δ in terms of the different requirement. Furthermore, a new method which can estimate the structural parameter α and F of the local model is proposed, the simulation result demonstrates the validity of this new method. However, since the variation of input gain α can impact the robustness of the system, some further researches need to be done to enhance the robustness of this method.

Moreover, except some modifications on the current method, some other control techniques are added to the model-free control. As the positioning stage often executes repetitive tasks, iterative learning control is combined to compensate for repetitive error and disturbances. Then a feedforward model which can predict the required force for pre-sliding motion is added to cancel the nonlinear pre-sliding friction and reduce the control effort. The effectiveness and validity of this simple new control method are verified through the simulation and real experiment.

6-2 Future work

Some of the challenges are discussed in this thesis. However, there is some work to do in the future.

(1) Further research on robustness of structural parameter estimation methods

The method for estimation of the structural parameter α has been proposed in this thesis. As can be seen in the simulation, the input gain α varies in a big range which probably results in the instability of the system. Thus it is necessary to bound α in a reasonable range to enhance the robustness of the new method.

(2) Research on the extension of the linear local model to a more complex model

Though good results have been obtained by this method, some further research on the extension of the current two-parameter linear local model is necessary. The simple local model, on the one hand can be easily estimated, but on the other hand loses its accuracy. If we make use of a more complex model of which both the simplicity and accuracy factors are taken into the consideration, the performance of model-free control will be further improved.

(3) Explorations for the combination of other new control methods and model-free control

Model-free control can be regarded as a feedforward control plus a feedback control. For simplicity, PID is selected to connect with a feedforward compensator. However, further explorations on the combination of other advanced control methods and model-free control are of great interest. The introduction of other advanced control technique to model-free control will improve the performance of the current model-free control method.

(4) Apply model-free control to different applications

As a newly proposed control method, model-free control is still continuously progressing. Thus applying this method to different applications and systems is a meaningful thing. As previously mentioned, the first order model-free control is likely to perform poorly in air bearing positioning systems due to the lack of the first-order term in its model. We can yield more findings by the application and experimental process.

Appendix A

Hardware specification

Table A-1: 2D encoder specifications

2D encorder specifications	
Range	$40 \times 45\ mm$
Resolution	$0.3nm$
Max tracking velocity	$4m/s$
Distance encoder head-grid	$12mm$
Updata rate	2MHz

Table A-2: Measured coil and magnet specifications

Coil and magnet specifications	x-actuator
Resistance R	12.8 Ω
Inductance L	490 μH
No. Windings	124
Magnet dimensions	$20 \times 6 \times 3\ mm$
Magnet remanent flux density B_r	1.43T
Average flux density in air gap B_g	0.7-0.83T
Motor Constant k_t	1.47 N/A

Table A-3: Measured amplifier specifications

Item	Amplifier 1	Amplifier 2	Amplifier 3
Gain $[A/V]$	0.243	0.241	0.244
Offset $[mA]$	0.3	1.3	0.7
Noise level at $10KH_z$	4	4	4

A-1 2D encoder datasheet

NanoGrid Planar Encoder System: Model A (High Resolution)

PRODUCT DESCRIPTION

The NanoGrid® Planar Encoder System is used to measure 2-dimensional ultra-precise planar displacements. NanoGrid is an XY grid-based encoder system that avoids the turbulence effects which are commonly encountered with laser interferometers or the Abbe errors associated with separate linear scales. NanoGrid captures the precision of laser interferometry within the manufacturing process of the grid and packages it in a lower cost, more usable and rugged format.

The XY encoder, or grid, has a basic period of 10 microns in both the X and Y directions, and the metrology system generates a measurement period of 5 microns. The NanoGrid's patented tri-phase 90-element detector captures first order laser diffracted signals reflected from the grid. The three signals generated by the detector provide an unambiguous measurement of phase for extremely small movements.

The NanoGrid Model A metrology system is unique in a number of its features, but particularly in the high degree of accurate interpolation that it provides. The NanoGrid sensor and associated high resolution phase processor electronics provide 14 bits of interpolation, corresponding to a measurement resolution of 0.3nm.

Several standard grid sizes are available to meet the requirements of semiconductor equipment manufacturers and other customers. Custom grid sizes can also be purchased for an exact fit.

The standard position output signal is available in the form of a 32-bit parallel word or in A-quad-B format. Position data is also available over the PCI bus at rates up to 110kHz. Yaw (rotation about the axis perpendicular to the plane) can be measured by adding a second single-axis sensor head.

NanoGrid is an excellent choice for submicron ultra precision XY positioning or as a calibration tool for high precision machine tools and stages.

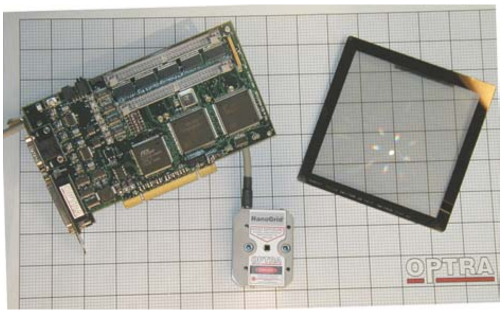

NanoGrid System Components. High Resolution Processor Board, NanoGrid Sensor Head and Grid Encoder. A 100mm grid is shown; other sizes are available upon request.

ADVANTAGES

- Sub-nanometer position resolution
- Measurement repeatability of ≤5 nm
- Reduced Abbe Error
- Insensitivity to turbulence and atmospheric pressure changes
- Small footprint & low moving mass
- Vacuum compatible units available
- Easy to install; stress-relieved grid mounting available.
- 12 mm clearance between grid and sensor head
- Low sensitivity to alignment errors
- Full technical support; customization available
- High-speed operation

OPTRA, Inc.
461 Boston St. Topsfield, MA 01983
978-887-6600 FAX: 978-887-0022
info@optra.com or www.optra.com

A-2 2D encoder datasheet

OPTRA, Inc. 461 Boston St. Topsfield, MA 01983 978-887-6600 FAX: 978-887-0022

System Performance

Repeatability	±5nm
Accuracy *	See Plot
** For more information on NanoGrid system accuracy please visit www.optra.com*	
Maximum tracking velocity	4 meters/sec
Encoder to sensor head gap	12.0 ±0.05 mm
Measurement area (others available)	40×45mm, 150×150mm 210×210mm, 380×380mm
Operating temperature	+10C to +40C
Storage temperature	–20C to +50C

NanoGrid Sensor Head

Dimensions	23.5 × 47.0 × 60.5mm
Housing material	6061-T6 aluminum
Light source (690nm)	Class IIIb 35mW laser diode
Weight without cable	110gm
Interface cable	3 m cable, 15-pin connector

Two-Axis High-Resolution Processor

Resolution	LSB = 5µm ÷ 2^{14} ≈ 0.305 nm
Update rate/axis	(parallel out) 2MHz
Range	~1300 mm (32 bit rollover)
Data age @ parallel out	< 1.2µsec; stability < 25 nsec
Interfaces	25-pin test connector Two 60-pin parallel connectors 32-bit PCI bus: 33MHz @3.3 or 5V 15-pin HD to Sensor Head
Output format	32-bit parallel word (each axis)
A-quad-B	Edge rate, MHz: 2.5, 5, 10, 20 Resolution: 5µm÷2^N; N = 9 to 14; ≈0.3 to 39.1 nm Edge-rate & resolution selectable
Mechanical	PCI-compatible 32-bit PC board
Power (Does not include A-quad-B board)	+5VDC (+0.25/-0.13 V)@ 0.5 A; +12VDC ±0.5V @120 mA; –12VDC ± 0.5V @150 mA

NanoGrid Encoder

Pitch (mechanical/optical)	10 µm / 5µm
Soda-lime expansion coefficient:	7.0 × 10^{-6}/°C
Quartz (fused silica) expansion coeff:	0.7 × 10^{-6}/°C
Other materials available – consult factory	

System Components
The NanoGrid Model A System consists of a planar encoder (XY grid), sensor head with cable, and 2-axis hi-resolution processor board.

NanoGrid Encoder
The standard NanoGrid encoder is a 10 µm pitch, 2-dimensional diffraction grating on soda-lime glass. The XY grid can be attached to a metal ring with incorporated flexures that provides kinematic mounting with stress relief and ease of installation.

NanoGrid Sensor Head
The NanoGrid Sensor Head contains a single laser diode source and separate optical systems for making planar position measurements. Output signals from the Sensor Head go to the Processor.

Two-Axis High-Resolution Processor
The Two-Axis High-Resolution Processor is a full size, PCI-bus-compatible PC plug-in card. It supplies power to, and receives signals from the NanoGrid Sensor Head via an interface cable. After processing these signals, it generates 32-bit words which describe the position of the encoder relative to the NanoGrid Sensor Head. Binary (TTL) flags and board-mounted LED's indicate excess speed and low signal conditions. An A-quad-B output with selectable resolution is available as well as the parallel digital word. Diagnostic signals are available at the 25-pin test connector, and over the PCI bus.

Documentation Package
This package contains dimensional and tolerance information needed to properly locate the NanoGrid sensor head relative to the NanoGrid encoder, instructions for mounting the NanoGrid encoder, and an operating manual.

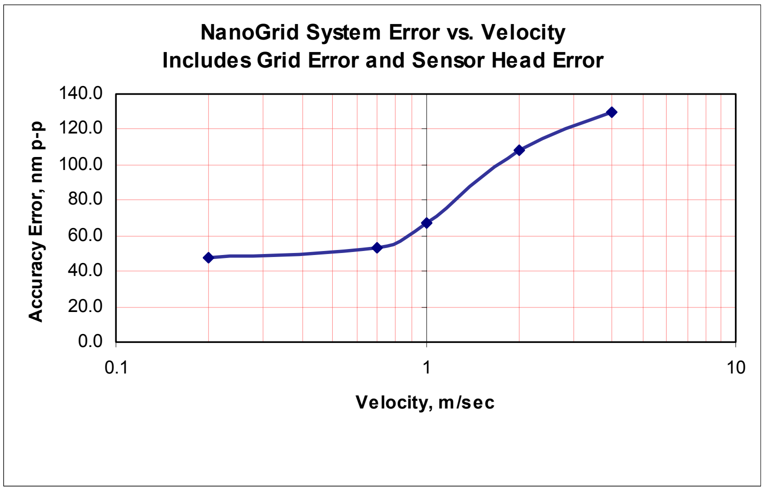

Bibliography

[1] P. Ouwehand, "Novel nanometer precision planar positioning stage using pre-sliding friction," 2015.

[2] M. Heertjes, T. Oomen, and D. Trumper, "Introduction to the special issue on control of high-precision motion systems: editorial," 2014.

[3] M. Inoue, "Positioning stage device exposure apparatus and device manufacturing method utilizing the same," Nov. 11 1997. US Patent 5,685,232.

[4] P. R. Dahl, "A solid friction model," tech. rep., DTIC Document, 1968.

[5] R. Leine, D. Van Campen, A. De Kraker, and L. Van Den Steen, "Stick-slip vibrations induced by alternate friction models," *Nonlinear dynamics*, vol. 16, no. 1, pp. 41–54, 1998.

[6] N. van Dijk, H. Nijmeijer, N. van de Wouw, and I. M. Dorrepaal, "Adaptive friction compensation of an inertia supported by mos2 solid-lubricated bearings," *Eindhoven University of Technology, Mechanical Engineering, Dynamics and Control Group, no. DCT*, vol. 6, p. 2005, 2005.

[7] Z. Jamaludin, H. Van Brussel, and J. Swevers, "Quadrant glitch compensation using friction model-based feedforward and an inverse-model-based disturbance observer," in *2008 10th IEEE International Workshop on Advanced Motion Control*, pp. 212–217, IEEE, 2008.

[8] P. Verboven, "Frequency-domain system identification for modal analysis," *Vrije Universiteit Brussel, Brussels*, 2002.

[9] M. Fliess, "Model-free control and intelligent pid controllers: towards a possible trivialization of nonlinear control?," *IFAC Proceedings Volumes*, vol. 42, no. 10, pp. 1531–1550, 2009.

[10] M. Fliess and C. Join, "Model-free control," *International Journal of Control*, vol. 86, no. 12, pp. 2228–2252, 2013.

[11] J. Wang, *Quadrotor analysis and model free control with comparisons.* PhD thesis, Université Paris Sud-Paris XI, 2013.

[12] M. Fliess, C. Join, and H. Sira-Ramirez, "Non-linear estimation is easy," *International Journal of Modelling, Identification and Control*, vol. 4, no. 1, pp. 12–27, 2008.

[13] J. Zehetner, J. Reger, and M. Horn, "A derivative estimation toolbox based on algebraic methods-theory and practice," in *2007 IEEE International Conference on Control Applications*, pp. 331–336, IEEE, 2007.

[14] J. Han, "From pid to active disturbance rejection control," *IEEE transactions on Industrial Electronics*, vol. 56, no. 3, pp. 900–906, 2009.

[15] Y. X. Su, B. Y. Duan, C. H. Zheng, Y. Zhang, G. Chen, and J. Mi, "Disturbance-rejection high-precision motion control of a stewart platform," *IEEE transactions on control systems technology*, vol. 12, no. 3, pp. 364–374, 2004.

[16] H. Tang and Y. Li, "Development and active disturbance rejection control of a compliant micro-/nanopositioning piezostage with dual mode," *IEEE Transactions on Industrial Electronics*, vol. 61, no. 3, pp. 1475–1492, 2014.

[17] P. Jiang, J.-Y. Hao, X.-P. Zong, and P.-G. Wang, "Modeling and simulation of active-disturbance-rejection controller with simulink," in *2010 International Conference on Machine Learning and Cybernetics*, 2010.

[18] J. Villagra and C. Balaguer, "A model-free approach for accurate joint motion control in humanoid locomotion," *International Journal of Humanoid Robotics*, vol. 8, no. 01, pp. 27–46, 2011.

[19] J. M. Rodriguez-Fortun, F. Rotella, J. Alfonso, F. Carrillo, and J. Orus, "Model-free control of a 3-dof piezoelectric nanopositioning platform," in *52nd IEEE Conference on Decision and Control*, pp. 342–347, IEEE, 2013.

[20] J. Zehetner, J. Reger, and M. Horn, "Echtzeit-implementierung eines algebraischen ableitungsschätzverfahrens (realtime implementation of an algebraic derivative estimation scheme)," *at-Automatisierungstechnik*, vol. 55, no. 11, pp. 553–560, 2007.

[21] H. Thabet, M. Ayadi, and F. Rotella, "Ultra-local model control based on an adaptive observer," in *2014 IEEE Conference on Control Applications (CCA)*, pp. 122–127, IEEE, 2014.

[22] H. Thabet, M. Ayadi, and F. Rotella, "Towards an ultra-local model control of two-tank-system," *International Journal of Dynamics and Control*, vol. 4, no. 1, pp. 59–66, 2016.

[23] Q. Zheng and Z. Gao, "On practical applications of active disturbance rejection control," in *Proceedings of the 29th Chinese control conference*, pp. 6095–6100, IEEE, 2010.

[24] P. Dupont, B. Armstrong, and V. Hayward, "Elasto-plastic friction model: contact compliance and stiction," in *Proceedings of the American control conference*, vol. 2, pp. 1072–1077, 2000.

[25] S.-W. Yu, "Enhanced iterative learning control with applications to a wafer scanner system," 2011.

[26] W. Qian, S. Panda, and J.-X. Xu, "Speed ripple minimization in pm synchronous motor using iterative learning control," *IEEE Transactions on Energy Conversion*, vol. 20, no. 1, pp. 53–61, 2005.

[27] D. Wang, "On d-type and p-type ilc designs and anticipatory approach," *International Journal of Control*, vol. 73, no. 10, pp. 890–901, 2000.

[28] K. L. Moore, "An observation about monotonic convergence in discrete-time, p-type iterative learning control," in *Intelligent Control, 2001.(ISIC'01). Proceedings of the 2001 IEEE International Symposium on*, pp. 45–49, IEEE, 2001.